Andean Geology 44 (2): 147-178. May, 2017
doi: 10.5027/andgeoV44n2-a03

Andean Geology
www.andeangeology.cl

Geochemistry of Permian to Triassic igneous rocks from northern Chile (28º-30º15'S): Implications on the dynamics of the proto-Andean margin

Felipe Coloma[1], Ximena Valin[2], *Verónica Oliveros[2], Paulina Vásquez[1], Christian Creixell[1], Esteban Salazar[1], Mihai, N. Ducea[3,4]

[1] *Servicio Nacional de Geología y Minería, Avda. Santa María 0104, Santiago, Chile.*
felipe.coloma@sernageomin.cl; paulina.vasquez@sernageomin.cl; christian.creixell@sernageomin.cl; esteban.salazar@sernageomin.cl

[2] *Departamento Ciencias de la Tierra, Universidad de Concepción, Víctor Lamas 1290, Casilla 160-C, Concepción, Chile.*
voliveros@udec.cl; ximena.valin@gmail.com

[3] *Department of Geosciences, University of Arizona, Tucson, AZ 85721, USA.*
ducea@email.arizona.edu

[4] *Universitatea Bucuresti, Facultatea de Geologie Geofizica, Strada N. Balcescu Nr 1, Bucuresti, Romania*

** Corresponding author: voliveros@udec.cl*

ABSTRACT. Permian to Triassic igneous rocks cropping out in the Coastal and Frontal cordilleras in northern Chile between 28º00'S and 30º15'S have long been interpreted to represent products of magmatism related to an extensional tectonic setting, either as the result of crustal anatexis or asthenospheric mantle decompression melting, in a passive continental margin. Eighty-six samples of plutonic (61) and volcanic (25) rocks from this region are characterized petrographically and geochemically. They are Permian to Early Jurassic in age, but the majority of the studied rocks correspond to the Lower to Middle Triassic Chollay Plutonic Complex, the volumetrically most important unit in the area. The rock samples have features typical of magmas derived from flux-induced melting of a depleted mantle such as: broad range of petrographic composition with predominance of intermediate to acid members, highly porphyrytic volcanic rocks, magnetite as the Fe-Ti oxide mineral phase, enrichment in LILE over HFSE, marked depletion in Nb, Ta, Ti, and P and moderate to no negative Eu anomalies. Few of the studied rock samples (<10%) have alkaline signature and trace element contents representative of anorogenic magmatism. In this work, we propose that subduction of an oceanic plate beneath the South American continent is responsible for the evolution of the margin from the Permian to Early Jurassic, at the studied latitudes. A preliminary interpretation of the margin architecture of the Andean margin from the Permian to the Triassic would be that the Chanchoquin and Chollay plutonic complexes represent the roots of a magmatic arc developed from the Permian to the Middle or early Late Triassic, whereas the Guanaco Sonso and Pastos Blancos formations would be the shallower parts of such arc. The La Totora Formation and some volumetrically minor Upper Triassic intrusive units represent magmatic products with alkaline signatures, which developed immediately before the establishment of the magmatic arc in the present-day Coastal Cordillera (during the Rhaetian to Early Jurassic).

Keywords: Triassic, Subduction, Pre-andean, Frontal cordillera, Geochemistry.

RESUMEN. Geoquímica de rocas ígneas Permo-Triásicas del norte de Chile (28º-30º15'S): Implicancias en la dinámica del margen pre-Andino. Las rocas ígneas del Permo-Triásico que afloran en las cordilleras de la Costa y Frontal en el norte de Chile, entre los 28º00' S y 30º15' S han sido interpretadas históricamente como productos de magmatismo asociados a un ambiente extensional, como el resultado de un proceso de anatexis cortical o bien fusión de manto astenosférico, en un margen pasivo. Se analizaron 86 muestras, de las cuales 61 corresponden a rocas plutónicas y 25 a rocas volcánicas, a las que se les hizo una caracterización petrográfica y geoquímica. Son de edad pérmica a jurásica inferior, pero la mayoría de las muestras de rocas analizadas corresponden al Complejo Plutónico Chollay, de

edad Triásico Inferior-Medio, siendo la unidad más importante en el área de estudio. Las muestras analizadas tienen características típicas de magmas derivados de fusión de un manto empobrecido como: amplio rango composicional con predominio de los componentes intermedio a ácidos, rocas volcánicas altamente porfídicas, magnetita como fase mineral principal de Fe-Ti, enriquecimiento en elementos LILE sobre HFSE, empobrecimientos en Nb, Ta, Ti y P, y moderada a inexistente anomalía negativa de Eu en las rocas estudiadas; algunas (<10%) tienen signatura alcalina y contenidos de elementos traza representativos de magmatismo anorogénico. En este trabajo, se propone que la subducción de una placa oceánica bajo el continente de Sudamérica es responsable de la evolución del margen entre el Pérmico y el Jurásico Inferior, a las latitudes estudiadas. Una interpretación preliminar de la arquitectura del margen Andino desde el Pérmico al Triásico puede ser que los complejos plutónicos Chanchoquín y Chollay representen las raíces de un arco magmático desarrollado entre el Pérmico y el Triásico Medio a Superior, mientras que las formaciones Guanaco Sonso y Pastos Blancos podrían ser porciones más superficiales de este arco. La Formación La Totora y algunos cuerpos menores de intrusivos del Triásico Superior representan productos con signaturas alcalinas, los que se desarrollaron inmediatamente antes del establecimiento del arco magmático en la actual cordillera de la Costa (durante el Raetiano al Jurásico Inferior).

Palabras clave: Triásico, Subducción, Pre-andino, Cordillera frontal, Geoquímica.

1. Introduction

The Permian to Triassic is a controversial period for the southwestern Gondwana margin evolution since it is thought to represent a significant magmatic lull that resulted from lack of subduction after the orogenic collapse following the Permian "San Rafael" orogenic event (Nasi *et al.,* 1990; Mpodozis and Ramos, 1989; Mpodozis and Kay, 1992). The magmatic sources would have changed significantly, decreasing the crustal component, between the Late Permian and the Early Jurassic. This change, which occurred during the Triassic, is explained by some authors as the response to a shift from subduction in a compressive setting to an extensional continental rift-related tectonic setting due to Pangea breakup (Mpodozis and Kay, 1992; Hervé *et al.,* 2014), or as extensional deformation in the overriding plate, in a continuous subduction setting (Vásquez *et al.,* 2011; Poma *et al.,* 2014; Del Rey *et al.,* 2016).

In the Coastal and Frontal cordilleras of north-central Chile (the latter being that part of the Andes along the Chile-Argentina border between 28º20' and 31º S that features uplifted Paleozoic basement blocks), successive Cretaceous to Miocene deformation fronts within the current flat-subduction segment of the Andes have generated both thin- and thick-skinned deformation in a fold-and thrust belt (Moscoso and Mpodozis, 1988; Martínez *et al.,* 2012), exposing large portions of late Paleozoic and early Mesozoic basement between 27º00' and 30º00'S (Ribba *et al.,* 1988; Salazar *et al.,* 2013; Hervé *et al.,* 2014). Thus, the geological record representing the Gondwana and Early Andean stages of the evolution of the South American margin are well exposed, although highly deformed. In particular, units cropping out in the Precordillera and Frontal Cordillera of northern Chile between 28°00' and 29°30', are a good record of this key time frame prior to the Andean subduction.

In Argentina, the Late Permian to Triassic period is characterized by the widespread magmatism represented by the Choiyoi group, whose origin had been attributed to crustal anatexis due to lithospheric extension associated to an orogenic collapse (Llambías and Sato, 1990; Llambías *et al.,* 1993). Acid explosive volcanism is well documented until the Early Triassic and followed by sedimentary rift deposits with basaltic rocks of anorogenic affinities, in the Cuyo and Ichigualasto basins (Ramos and Kay, 1991).

The geological cartography of northern Chile between 27°00' and 30°00' has been updated over the past decade with works performed, at 1:100.000 scale, by the Servicio Nacional de Geología y Minería (SERNAGEOMIN) (Welkner *et al.,* 2006, Arévalo and Welkner, 2008; Moscoso *et al.,* 2010; Salazar *et al.,* 2013; Creixell *et al.,* 2012; Creixell *et al.,* 2013; Martínez *et al.,* 2015; Ortiz and Merino, 2015; Salazar and Coloma, 2016). These works include large geochronological databases in addition to refined litho stratigraphic unit definitions. In particular, the Late Paleozoic to Triassic rock units has been significantly modified, incorporating several new units and redefining those previously known. Even though extensive outcrops of acidic volcanic and subvolcanic rocks from the Late Carboniferous to the Permian are exposed in the Precordillera and Frontal Cordilleras, and interpreted as equivalents to the Choiyoi Group. The Triassic rock units are

more diverse and include large plutonic complexes, explosive volcanic sequences of dacitic to rhyolitic composition, continental to marine sedimentary sequences with minor volcanic component, and volcanic sequences of basaltic-andesite to rhyolitic composition (Reutter, 1974; Nasi *et al.,* 1990; Salazar *et al.,* 2013; Ortiz and Merino, 2015; Salazar and Coloma, 2016). Thus, the development of a continental rift phase in the South American plate during the Triassic is not a straightforward from the geological record in northern Chile between 27º and 30º S. Furthermore, extensive geochemical data from the Triassic units is lacking, precluding a tectonic interpretation of the magmatism from its chemical signature.

In this paper, we present new petrographical and geochemical data for several, Late Paleozoic to Triassic, plutonic and volcanic units cropping out in the Coastal (28º00' S-29º30' S) and Frontal cordilleras of northern Chile (28°30' S-30°15' S). The geochronology of these units has been presented elsewhere (Creixell *et al.,* 2012; Valin, 2014; Vallejos, 2014; Salazar *et al.,* 2013; Creixell *et al.,* 2016; Ortiz and Merino, 2015; Salazar and Coloma, 2016). The new data allow us to revise previous models for the tectonic setting of the Paleozoic to Triassic magmatism, its sources and processes of generation.

2. Geological Setting

In the Coastal Cordillera (28º-29º S, Fig. 1), the Paleozoic basement is represented by the Devonian to Permian Punta de Choros Metamorphic Complex, composed by micaschists and metabasites (Creixell *et al.,* 2012) and Chañaral Epimetamorphic complexes, which consists mainly of metaturbidites and metasedimentary rocks (Godoy and Lara, 1998) and the Carboniferous to Permian Llano de Chocolate Beds (Creixell *et al.,* 2012, 2016). The latter is a sedimentary rock sequence, mainly continental, deposited in a delta environment with proximal volcanic deposits (Creixell *et al.,* 2016). These Paleozoic units are unconformably overlaid by Triassic rocks of the Canto del Agua Formation, a geographically restricted sedimentary sequence, and the volcanic Jurassic rocks included in the La Negra Formation, and intruded by several plutonic complexes ranging in age from the Upper Triassic to the Lower Cretaceous (Welkner *et al.,* 2006; Arévalo and Welkner, 2008; Creixell *et al.,* 2012). Among the older Mesozoic intrusives are the Carrizal Bajo Plutonic complex, a suite of diorites, quartz diorites, granodiorites and granites bounded by synplutonic normal faults and an age range between 208 and 206 Ma, the Algodones Granite composed of monzogranites and granodiorites of 203-199 Ma and surrounded by amphibole mylonites (Welkner *et al.,* 2006; Arévalo and Welkner, 2008; Creixell *et al.,* 2012) and the Quebrada La Vaca Tonalite, composed of tonalites and quartz diorites ranging in age from 193 to 191 Ma (Welkner *et al.,* 2006; Creixell *et al.,* 2012).

Several Paleozoic and Mesozoic units are recognized in the Frontal Cordillera, the most relevant of which to the present study are listed in Table 1. The Permian and Triassic plutonic units have a distinct spatial distribution along the Frontal Cordillera, as two parallel, roughly N-S trending, belts. The western belt comprises Pennsylvanian to Cisularian granitoids of the Guanta and Chanchoquin plutonic complexes that intrude Late Devonian to Missisipian metamorphic rocks and penecontemporaneous volcanic deposits (Fig. 1). The eastern belt is composed mainly by outcrops of the Chollay Plutonic Complex, intruding Devonian metasediments, Carboniferous granitoids, Permian metamorphic rocks and tonalites, and penecontemporaneous volcanic deposits with minor components of Permian intrusives. In between the two belts, scattered outcrops of Carboniferous granitoids and high-grade gneiss and metaplutonic rocks are found (Salazar *et al.,* 2013; Ortiz and Merino, 2015; Salazar and Coloma, 2016) (Fig. 1).

The Guanta Plutonic Complex (Ortiz and Merino, 2015), equivalent to the Guanta unit of Nasi *et al.* (1985), is composed of leuco to mesocratic, coarse to medium-grained, partly foliated, biotite and amphibole tonalites and granodiorites, ranging in age from 300 to 280 Ma (Nasi *et al.,* 1985; Hervé *et al.,* 2014; Ortiz and Merino, 2015). In continuity to the north, the Chanchoquín Plutonic Complex is a suite of medium to coarse grained granitoids composed of two-mica granodiorites, monzogranites, biotite and amphibole tonalites and diorites, that ranges from 297 to 285 Ma in age (Salazar *et al.,* 2013). The Quebrada El Pintado Tonalites are small foliated plutonic bodies and correspond to tonalites and granodiorites of amphibole and biotite, of Middle Permian age (272-266 Ma, Salazar and Coloma, 2016). All the aforementioned units were previously assigned to

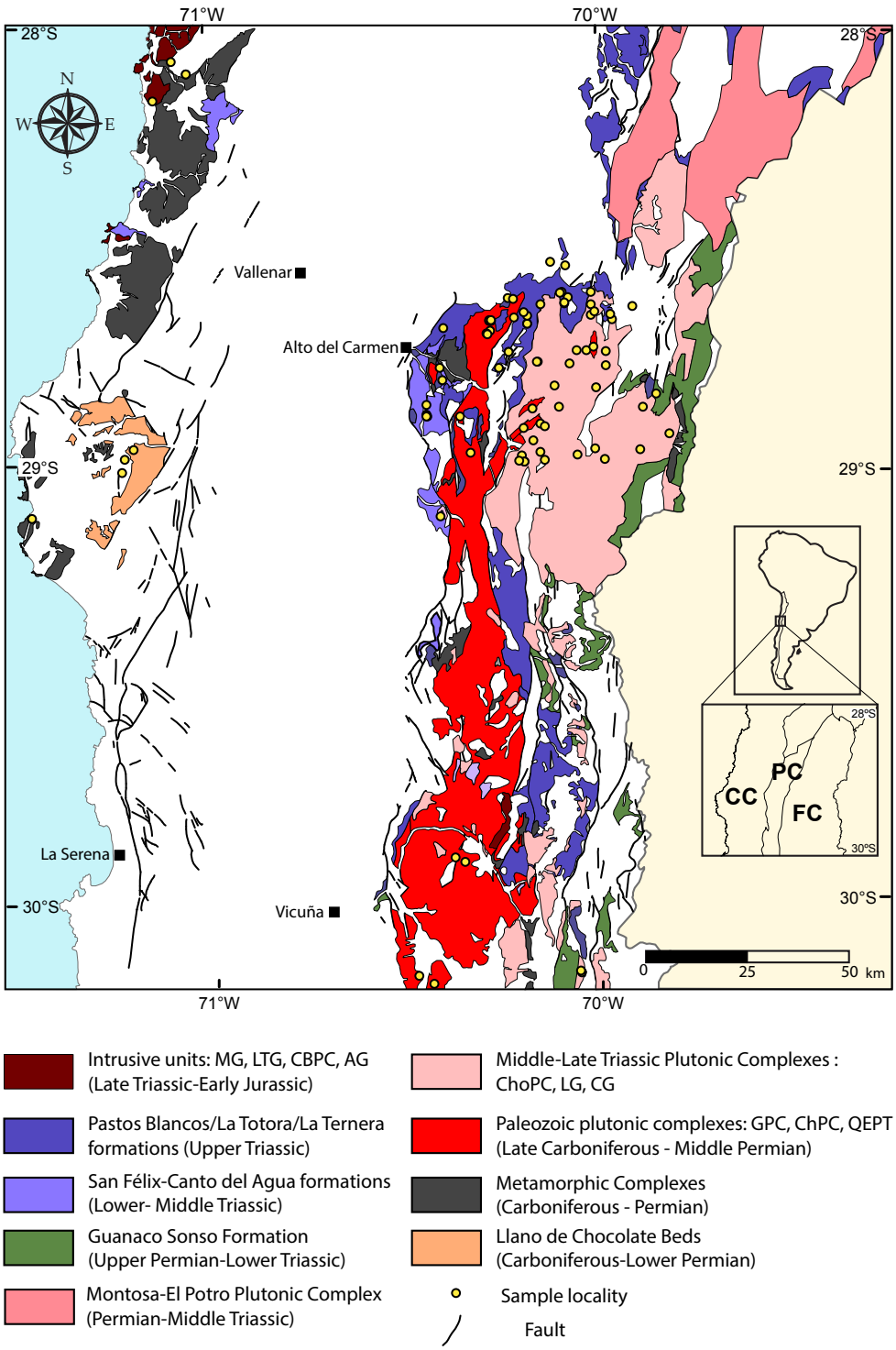

FIG. 1. Simplified geological map of the studied region including sample location. **GPC:** Guanta Plutonic Complex, **ChPC:** Chanchoquín Plutonic Complez, **QEPT:** Quebrada el Pintado Tonalites, **ChoPC:** Chollay Plutonic Complex, **LG:** La Laguna Gabbro, **CG:** Colorado Syenogranite, **MG:** Montegrande Granite; **LTG:** Los Tilos Pluton; **CBPC**: Carrizal Bajo Plutonic Complex; **AG:** Algodones Granite; **CC:** Coastal Cordillera, **PC:** Precordillera, **FC:** Frontal Cordillera.

the Elqui Superunit, an association of Carboniferous to Permian tabular coarse grained plutonic bodies believed to reflect significant crystallization depths (Nasi *et al.,* 1985). The Chollay Plutonic Complex, equivalent to the Chollay unit of Nasi *et al.* (1985), range in ages from 249 to 236 Ma and is composed of five different lithofacies, with medium to very coarse grained plutons that include gabbro-diorite, tonalite, syenogranite, granodiodiorite and monzogranite, being the two latter the most abundant (Salazar *et al.,* 2013; Salazar and Coloma, 2016). The Colorado syenogranite corresponds to a group of hololeucocratic, fine-grained to porphyritic plutonic bodies of characteristic reddish color, that range in age from 225 to 219 (Nasi *et al.,* 1985; Salazar *et al.,* 2013; Maksaev *et al.,* 2014). In the same geographic position as the Colorado syenogranite, several dioritic and granodioritic units have been lately described by Ortiz and Merino (2015), with an age of *ca.* 215 Ma. Other upper Triassic intrusive rocks are the La Laguna Gabbro, Montegrande Granite, Los Tilos Granodiorite (also called Los Tilos Pluton after Nasi *et al.,* 1990; Hervé *et al.,* 2014) and mafic dike swarms (Mpodozis and Cornejo, 1988; Martin *et al.,* 1999; Creixell *et al.,* 2009; Hervé *et al.,* 2014). All these units were assigned to the Ingaguás Superunit by Nasi *et al.* (1985).

One of the oldest stratified units is the Upper Permian- Lower Triassic Guanaco Sonso Formation which is unconformably overlain by the Upper Triassic Pastos Blancos Formation (Nasi *et al.,* 1990; Martin *et al.,* 1999; Ortiz and Merino, 2015; Salazar and Coloma, 2016). These units were originally assigned to the Pastos Blancos Formation (Nasi *et al.,* 1990) or to the Guanaco Sonso and Los Tilos Sequences of the Pastos Blancos Group (Martin *et al.,* 1999). They consist mainly of pyroclastic and volcanoclastic rocks, of intermediate to acidic composition with minor basalts, (Martin *et al.,* 1999; Salazar *et al.,* 2013; Ortiz and Merino, 2015; Salazar and Coloma, 2016), but they are also including coarse sandstones, conglomerates and epiclastic rocks. While rocks of the Guanaco Sonso Formation unconformably overlie Paleozoic metamorphic basement, the rocks of Pastos Blancos Formation rest over the Chollay Plutonic Complex and is in turn intruded by the Colorado syenogranites and dykes. The San Félix Formation is a 6,000 m thick clastic continental-marine rock succession of Triassic age (Reutter, 1974) that contains a few crystalline and lithic lapilli tuffs levels in some of its five members and basic to intermediate lavas in the uppermost member (Salazar *et al.,* 2013). Although the age range for this formation comprises the entire Triassic period, fossil content and U-Pb geochronology indicate that most of the sedimentation took place from the Lower to the Middle Triassic and only the uppermost member is Late Triassic in age, which is covered by and interfingers eastward with andesitic lavas of the La Totora Formation (Reutter, 1974; Salazar *et al.,* 2013). The La Totora Formation is a volcanic sequence composed of lavas and tuffs of basic and intermediate composition, ranging in age from 221 to 212 Ma (Reutter, 1974; Salazar *et al.,* 2013; Maksaev *et al.,* 2014; Salazar y Coloma, 2016). East from the outcrops of the San Félix Formation, La Totora Formation covers unconformably the Chollay Plutonic Complex and is covered by the marine Lower to Middle Jurassic rocks of the Lautaro Formation.

3. Samples and methods

The complete dataset includes eighty-six samples of plutonic (61) and volcanic (25) rocks (Table 1, Fig. 1) belonging to twelve different Paleozoic and Mesozoic units. For the purposes of this study, the volcanic rocks collected from outcrops of the uppermost member of the San Félix Formation are assigned to the La Totora Formation, according to the information given in the previous chapter. The lithologies of the selected samples are: basaltic, basaltic-andesite and dacitic lavas, crystal and lithic lapilli tuffs, granodiorites, tonalites, granites, gabbros and diorites. Sixty-five samples were collected during the geological mapping of the Precordillera and Frontal Cordillera between 28º30' and 29º00'S by a team of the Servicio Nacional de Geología y Minería (SERNAGEOMIN). The petrographic description and methods used in the geochemical analysis of these rock samples are detailed in Salazar *et al.* (2013) -they can be obtained from authors Coloma and Salazar upon request- and summarized here and in the following chapters. The remaining twenty-one samples were collected in the Coastal Cordillera and Precordillera between 28º S and 30º15' S for petrographic and geochemical analysis. The thin sections were analyzed under the polarized-light microscope for a textural and mineralogical characterization. The samples were crushed and fresh fragments handpicked under binocular microscope.

TABLE 1. GEOLOGICAL UNITS STUDIED IN THIS WORK WITH THEIR REPRESENTATIVE LITHOLOGIES AND AGE RANGE, ANALYZED SAMPLES FOR EACH UNIT AND THEIR ALTERATION DEGREE EXPRESSED AS % OF THE TOTAL VOLUME OF THE ROCK.

Unit	Samples	Lithologies	Alteration degree	Age range
Llano de Chocolate Beds	CPV-12-12, CPV-12-105, CPV-12-127	Rhyolite, Dacite, Rhyolitic tuff	0.24-0.8	318-285 Ma[1]
Chanchoquín Plutonic Complex and Guanta Unit	ST-04t, CT-310t, CT-311t, CT-312t, CT-333t, CT-340t, CT-91t, ST-70t, ST-71t, CT-236t, CT-334t, CT-337t, 07-15	Tonalite, Granodiorite	0.00-0.16	296-285 Ma[2]
Upper Permian Dike	ST-69t	Undetermined	0.1	-
Quebrada del Pintado Tonalites	CT-160t, CT-202t, CT-296t, ST-97t	Tonalite	0.02-0.08	272-259 Ma[2]
Guanaco Sonso Formation	CT-213t, CT-216t, ST-13t, ST-14t, CT-286t	Basalt, Basaltic Andesite, Dacite, Rhyolite	0.13-0.35	265-240 Ma[2]
La Laguna Gabbro	07-10, 07-11	Gabbro	0.01-0.02	255 Ma[3]
Chollay Plutonic Complex (Granodiorite)	CT-228t, ST-16t, CT-19t, CT-237t, CT-284t, ST-160t, CT-191t, CT-19Bt, CT-154t	Granodiorite	0.015-0.17	247-237 Ma[2]
Chollay Plutonic Complex (Monzogranite)	SCL-02t, CT-146At, CT-158t, CT-161t, CT-196t, CT-199t, CT-233t, CT-289t, CT-290t, CT-291t, CT-294t, CT-303t, ST-80t, ST-98Bt, ST-17t	Monzogranite	0.03-0.12	247-233 Ma[2]
Chollay Plutonic Complex (Tonalite)	SCL-09t, CT-164t, CT-167t, CT-173t, CT-250t, CT-255t, CT-300t, CT-35t	Tonalite	0.04-0.27	237-234 Ma[2]
Chollay Plutonic Complex (Gabbro-Diorite)	CT-193t	Diorite	0.11	249-242 Ma[2]
San Félix Formation	CPV-12-38, CPV-12-49b,CT-75At, ST-212At	Lithic tuff, Andesitic tuff, Tuff	0.1-0.7	254-212 Ma[2, 4]
Upper Triassic dike	CT-74t		0.4	-
Colorado Syenogranite	SCL-14t, ST-9t	Syenogranite	0.05-0.09	229-219 Ma[2]
La Totora Formation	ST-93At, ST-196t, ST-11t, ST-19t, CPV-12-23, CPV-12-24, CPV-12-60, SCL-26t, ST-62t, ST-175t, ST-43t	Andesitic tuff, Rhyolithic tuff, Andesite, Basalt, Tuff, Rhyolite, Rhyolithic tuff	0.08-0.89	221-210 Ma[2, 5]
Montegrande Granite	07-07, 07-06	Granite, Granodiorite	0.01	215 Ma
Los Tilos Pluton	07-13	Granodiorite	0.01	215 Ma
Carrizal Bajo Complex	CPV-12-91A, CPV-12-91B, CPV-12-93	Diorite, Tonalite, Granodiorite	0.05-0.23	208-206 Ma[6]
Algodones Granite	CPV-12-92	Diorite	0.4	203-199 Ma[6]

[1]Creixell *et al.* (2016); [2]Salazar *et al.* (2013); [3]Hervé *et al.* (2014); [4]Vallejos (2014); [5]Maksaev *et al.* (2014); [6]Arévalo and Welkner (2008).

The selected fragments pulverized under 60 μm for chemical analyses of major and trace elements. Major element contents were determined through XRF (X rays fluorescence) whereas trace elemental concentrations were determined on a quadrupole single collector ICP-MS at the Geosciences Department of the University of Arizona. Analytical techniques, sample preparation procedures and standards were previously described in Chapman *et al.* (2015) and Rossel *et al.* (2013).

U-Pb geochronology of zircons was conducted by LA-MC-ICP-MS at the Arizona LaserChron Center (Gehrels *et al.,* 2008). The analyses involve ablation of zircon with a New Wave/Lambda Physik DUV193 Excimer laser (operating at a wavelength of 193 nm) using a spot diameter of 25 or 35 μm. The ablated material is carried with helium gas into the plasma source of a GV Instruments Isoprobe, which is equipped with a flight tube of sufficient width that U, Th, and Pb isotopes are measured simultaneously. All measurements are made in static mode, using Faraday detectors for ^{238}U and ^{232}Th, an ion-counting channel for ^{204}Pb, and either Faraday collectors or ion counting channels for $^{208\text{-}206}$Pb. Ion yields are ~1 mV ppm^{-1}. Each analysis consists of one 20 s-integration on peaks with the laser off (for backgrounds), twenty 1 s-integrations with the laser firing, and a 30 s delay to purge the previous sample and to prepare for the next analysis. The ablation pit is ~15 μm in depth.

For each analysis, the errors in determining ^{206}Pb/^{238}U and ^{206}Pb/^{204}Pb result in a measurement error of ~1% (at 2σ level) in the ^{206}Pb/^{238}U age. The errors in measurement of ^{206}Pb/^{207}Pb and ^{206}Pb/^{204}Pb also result in ~1% (2σ) uncertainty in age for grains that are >1.0 Ga, but are substantially larger for younger grains due to low intensity of the ^{207}Pb signal. For most analyses, the crossover in precision of ^{206}Pb/^{238}U and ^{206}Pb/^{207}Pb ages occurs at ~1.0 Ga. Common Pb correction is accomplished by using the measured ^{204}Pb and assuming an initial Pb composition from Stacey and Kramers (1975) (with uncertainties of 1.0 for ^{206}Pb/^{204}Pb and 0.3 for ^{207}Pb/^{204}Pb). The measurement of ^{204}Pb is unaffected by the presence of ^{204}Hg because backgrounds are measured on peaks (thereby subtracting any background ^{204}Hg and ^{204}Pb), and because very little Hg is present in the argon gas. Interelement fractionation of Pb/U is generally ~20%, whereas fractionation of Pb isotopes is generally <2%. In-run analysis of fragments of a large Sri Lanka zircon crystal (generally every fifth measurement) with known age of 564±4 Ma (2σ error) is used to correct for this fractionation (see Gehrels *et al.,* 2008). The uncertainty resulting from the calibration correction is generally ~1% (2σ) for both ^{206}Pb/^{207}Pb and ^{206}Pb/^{238}U ages.

The reported ages are determined from the weighted mean of the ^{206}Pb/^{238}U ages of the concordant and overlapping analyses (Ludwig, 2003). The reported uncertainty (labeled "mean") is based on the scatter and precision of the set of ^{206}Pb/^{238}U or ^{206}Pb/^{207}Pb ages, weighted according to their measurement errors (shown at 1σ). The systematic error, which includes contributions from the standard calibration, age of the calibration standard, composition of common Pb and U decay constants, is generally ~1-2% (2σ).

4. Petrography of the plutonic and volcanic rocks

The petrography of the studied samples was carried out mainly in thin sections, in which the main mineralogy, both primary and secondary, was distinguished. Some images from the thin sections are detailed in figure 2, and the details of these descriptions are in the Appendix 1.

4.1. Llano de Chocolate Beds

In this unit, the volcanic and pyroclastic rocks are interbedded in the dominantly sedimentary sequence (Vallejos, 2014; Creixell *et al.,* 2016) and they correspond to dacitic lavas and crystalline lapilli tuffs. The dacites have porphyrytic texture, slightly seriated, with felsitic groundmass. The phenocrysts correspond to reabsorbed quartz, plagioclase and biotite. Alteration minerals represents up to 5% of the rock, with calcite and clay minerals replacing plagioclase, and biotite is replaced by epidote and chlorite. Quartz, biotite, calcite and sericite also occur in veinlets. The tuffs have fragmental texture with fiammes, and phenocrysts of quartz and plagioclase. Secondary calcite and biotite occur in veinlets.

4.2. Chanchoquín Plutonic Complex

The Chanchoquín Plutonic Complex is composed mainly of tonalites and granodiorites with minor monzogranites and diorites, the studied samples include only tonalitic and granodioritic lithologies. Granodiorites are fine to medium grained and contain

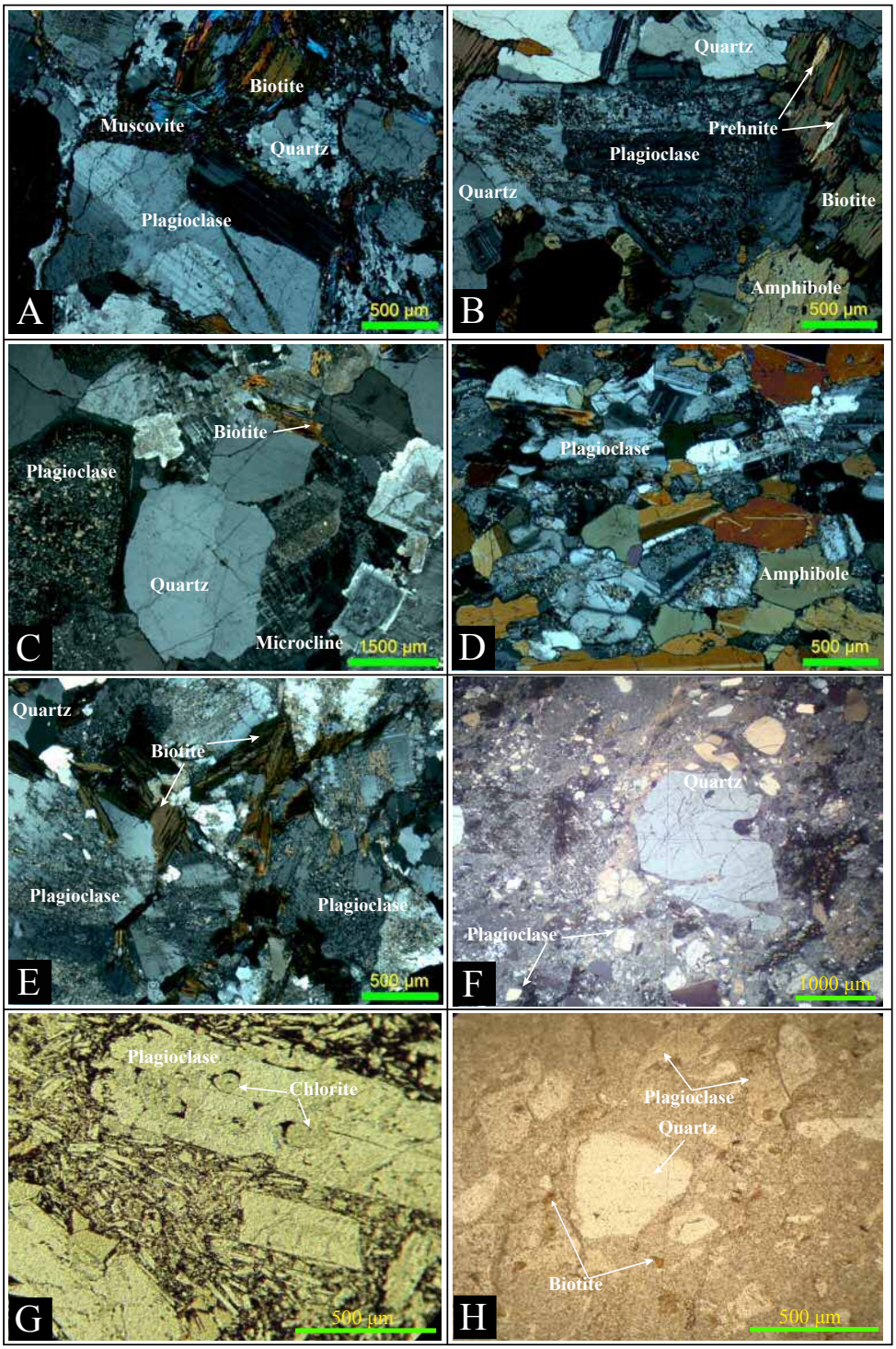

FIG. 2. Microphotographs of the most relevant lithologies of the studied units: **A.** Tonalite, Chanchoquín Plutonic Complex; **B.** Tonalite, Quebrada el Pintado Tonalites; **C.** Monzogranite, Chollay Plutonic Complex; **D.** Tonalite, Chollay Plutonic Complex; **E.** Granodiorite, Chollay Plutonic Complex; **F.** Dacite, Llano de Chocolate Beds; **G.** Andesitic clast in volcanic breccia, La Totora Formation; **H.** Crystalline tuff, San Félix Formation.

quartz with undulatory extinction, plagioclase, orthoclase, biotite and minor muscovite or amphibole; accessory minerals are Fe-Ti oxides (mainly magnetite) and sphene. Perthitic texture is observed in some feldspar crystals. These lithologies are slightly altered (less than 10% volume of the rock) with sericite replacing feldspars and prehnite and epidote replacing biotite. Tonalites are medium to fine grained, they contain quartz with undulatory extinction and polycrystalline, zoned plagioclase, orthoclase, biotite, muscovite, minor amphibole, with Fe-Ti oxides and apatite as accessory minerals. Alteration minerals are generally less than the 8% of the rock, but in three samples they reach the 15%, with sericite replacing feldspars and chlorite, epidote and prehnite replacing mafic minerals. At the outcrop scale, the rocks are foliated to variable degrees.

4.3. Los Tilos Granodiorite

This unit is characterized by the presence of cordierite in its mineralogy, with allotromorphic inequigranular texture; its composition varies between granite and granodiorite and is composed by quartz, alkali feldspar, plagioclase, biotite, white mica with slight deformation, and cordierite. The quartz has undulatory extinction and locally shows a granoblastic texture, biotite is altered to chlorite and epidote, and shows slight deformation, similar to the white mica.

4.4. Quebrada El Pintado Tonalites

The rocks of this units are grey fine to medium grained tonalites with local millimetric to centimetric foliation. They contain polycrystalline quartz with undulatory extinction, plagioclase, minor orthoclase, biotite, amphibole, pyroxene, muscovite and Fe-Ti oxides, with apatite as accessory minerals. Myrmekitic and perthitic textures are observed in the feldspars. Secondary mineral represent less than the 6% of the volume of the rock, with sericite replacing feldspars, and chlorite and epidote replacing biotite.

4.5. Guanaco Sonso Formation

This volcanic and sedimentary unit is volumetrically important in the Frontal Cordillera (Fig. 1) and it is composed mainly of dacitic to rhyolitic, partly welded tuffs and lava flows of basaltic, dacitic and rhyolitic composition. Minor sedimentary beds of volcarenites, siliciclastic laminated conglomerate and medium to coarse grained sandstone are found, along with scarce outcrops of lacustrine mudstone and chert. The main lithology is crystal and lithic-bearing vitric lapilli tuffs, with plagioclase, quartz and amphibole phenocrysts, acid volcanic fragments and pumice of millimetric to centimetric size.

4.6. Chollay Plutonic Complex

The Chollay Plutonic Complex is the largest intrusive unit in the studied area (Fig. 1) and it is composed mainly of monzogranite and granodiorite, along with diorite to gabbro, tonalite and syenogranite. The monzogranites are pink and coarse grained rocks, which contain quartz with undulatory extinction and locally polycrystalline, sometimes zoned plagioclase, orthoclase with perthitic texture, minor microcline, biotite, muscovite, with Fe-Ti oxides (mainly magnetite) and sphene as accessory minerals; alteration minerals represent up to the 10% of the rock volume, with sericite replacing feldspars, and chlorite and epidote replacing biotite. The granodiorites are grayish white, fine to medium grained rocks, with zoned plagioclase, quartz with undulatory extinction and locally polycrystalline, orthoclase with perthitic texture, biotite, amphibole and muscovite, with sphene, apatite and rutile as accessory minerals, the alteration minerals can reach 15% in volume of the rock, with mainly sericite replacing feldspars and chlorite replacing biotite, while epidote and prehnite are also observed replacing mafic minerals. The diorites and gabbros are dark grey, medium to fine grained rocks, they contain zoned plagioclase and variable amount of olivine and clinopyroxene, the latter with amphibole rims, minor biotite, and Fe-Ti oxides, apatite and rutile as accessory minerals; alteration minerals can reach 12% of the volume of the rock, with sericite replacing plagioclase and scarce chlorite and prehnite. The tonalites are medium to fine grained, grey rocks, contain quartz with undulatory extinction, zoned plagioclase, scarce orthoclase, biotite, hornblende, and Fe-Ti oxides (mainly magnetite), with apatite and sphene as accessory minerals, and alteration minerals represent between 7 to 25% of the total volume of the rock, with sericite replacing plagioclase (4-15%), chlorite replacing biotite and amphibole (3-12%) and disseminated epidote. The syenogranites are orange, medium grained rocks, contain scarce

plagioclase, ortoclase with pertitic texture, quartz with undulatory extinction, scarce Fe-Ti oxides, and zircon as accesory mineral.

4.7. Colorado Syenogranites

The lithologies in this plutonic unit vary from syenogranites to monzogranites with myrmekitic and graphic textures in the feldspars. The rocks are pink-orange, coarse to medium grained, with porphyric to phaneritic texture. Quartz with undulatory extinction, orthoclase, plagioclase and biotite are the main minerals with scarce opaque minerals (Fe-Ti oxides), and apatite and rutile as accessory minerals; alteration is weak and secondary minerals phases represent less than the 6% of the total volume of the rock, with sericite replacing plagioclase, chlorite replacing biotite and disseminated epidote.

4.8. San Félix Formation

The pyroclastic deposits are interbedded in the mainly siliciclastic rock sequence (Reutter, 1974; Ribba, 1985; Salazar *et al.,* 2013; Vallejos, 2014), and they correspond to centimeter thick beds of lapilli and ash tuffs. The volcanic rocks have fragmental texture and locally eutaxitic, silicic alteration affected the matrix and plagioclases phenocrysts are replaced by sericite and clays, fine veins filled with sericite, biotite and quartz crosscut the rock.

4.9. Montegrande Granite

The Montegrande granite is an NNW elongated intrusive with an area of *ca.* 16 km^2 (Parada, 1984). The granite is allotriomorphic inequigranular and is composed by alkali feldspar, quartz, plagioclase and minor amphibole, clinopyroxene, biotite and white mica. Alkali feldspar is anhedral and perthitic, while amphibole is interstitial, anhedral and often includes oxidized pyroxene, biotite and white mica are also interstitial. Locally, the amphibole is completely replaced by chlorite with minor biotite. The plagioclase is subhedral, with minor secondary sericite and often is rimmed by albite.

4.10. La Laguna Gabbro

It consists of small stocks with few hundreds of meters in diameter (Mpodozis and Cornejo, 1988, this work). The gabbros are coarse-grained with hypidiomorphic inequigranular texture with plagioclase, instersticial clinopyroxene, orthopyroxene, opaque minerals, and minor quartz and instersticial orthoclase. Locally, the rocks exhibit graphic texture. Clinopyroxene could be present as reaction rims which enclose opaque minerals. The alteration in these rocks is scarce, pyroxenes are altered to chlorite, epidote and opaque minerals whereas plagioclase are slightly altered to sericite.

4.11. La Totora Formation

This volcanic unit is composed by andesitic lava flows, volcanic breccias and a tuff level interbedded in the sequence. The lavas are reddish-violet andesites and basalts, with aphanitic to slightly porphyrytic texture, occasional vesicles and amygdales. The phenocrysts correspond to pyroxene and plagioclase with sieve texture, and the groundmass is hyalopilitic, locally intergranular, with plagioclase, pyroxene and olivine. The glass is altered to chlorite and Fe-Ti oxides. Secondary minerals represent up to 15% of the rock, with clay minerals, epidote and calcite replacing plagioclase, calcite in microveins, calcite and zeolite filling vesicles. The breccias are andesitic in composition. The clasts represent 15 to 40% of the total volume. They are lavas with porphyric and hyalophyric textures, plagioclase phenocryst (sieve textures) and glass, replaced by chlorite and Fe-Ti oxides. The matrix is similar in composition. The rocks are altered to calcite, quartz and clay minerals. Calcite is replacing plagioclase phenocryts and fill veinlets with quartz.

4.12. Carrizal Bajo Plutonic Complex and Algodones Granite

These plutonic bodies have a rather restricted distribution in the Coastal Cordillera (Welkner *et al.,* 2006; Arévalo and Welkner, 2008) (Fig. 1). The samples of the Algodones granite correspond to medium grained quartz diorites, with plagioclase, quartz, clinopyroxene and biotite. These lithologies are slight to strongly altered (5 to 40% vol), chlorite and amphibole replace clinopyroxene, epidote and chlorite replace biotite and plagioclase crystals are replaced by sericite and clay minerals. The samples of the Carrizal Bajo Plutonic Complex correspond to medium to fine grained, equigranular biotite

tonalites and granodiorites, and amphibole tonalite. They are slight to moderately altered, with chlorite and epidote replacing mafic minerals, and sericite and clay minerals replacing feldspars.

4.13. Dikes

They are hypabisal rocks with subophitic texture and basaltic-andesitic to andesitic in composition. The phenocrysts are principally plagioclase, with moderate alteration to sericite and clay minerals, Fe-Ti oxides and pyroxene, which is often altered to amphibole and chlorite.

5. Geochronological results and interpretation

Isotope chronology data have been published elsewhere for most of the studied rock units (see Martin *et al.,* 1999; Welkner *et al.,* 2006; Salazar *et al.,* 2013; Hervé *et al.,* 2014; Creixell *et al.,* 2016; Ortiz and Merino, 2015; Salazar and Coloma, 2016) and summarized in Table 1. In this work, four samples of small intrusive rock units were selected for U-Pb dating in igneous zircons (Fig. 3). The detailed results are listed in the Appendix 2.

One sample from the Guanta unit (O7-15), equivalent to the Chanchoquín Plutonic Complex, displays an age distribution pattern with a single-peak, for which the best estimated age is 297.0±4.0 Ma. One sample from a body assignated to Los Tilos pluton (O7-13) also yielded a single-peak age distribution pattern with a best estimated age of 290.3±3.0 Ma. In both cases, there are no discordant ages from individual grains. The age of the Guanta unit agrees with previous reported data (Nasi *et al.,* 1985; Hervé *et al.,* 2014; Maksaev *et al.,* 2014). In contrast, the Los Tilos pluton has been before assigned to the Ingaguás Superunit (Nasi *et al.,* 1985) and dated at 215.6±1.9 Ma (Hervé *et al.,* 2014) discordant with the result obtained in this work (290.3±3.0 Ma). Given that there are no younger single-grain ages, either concordant or discordant, in the analyzed sample, it is difficult to discard the result obtained for sample O7-13, but it is possible that it does not belong to the Los Tilos Pluton since the other data point to a Late Triassic rather than Early Permian age.

On the other hand, sample O7-07 from the Montegrande Granite yielded a best estimated age of 214.6±1.5 Ma, with one single grain age of 260.3±25.2 Ma, suggesting possible assimilation of older crustal rocks during magma generation or evolution. This age is in agreement with the geochronological data previously reported, which range between 192±11 and 215.6±1.4 Ma (Brook *et al.,* 1987; Hervé *et al.,* 2014). In the case of the La Laguna Gabbro (sample O7-11), crustal assimilation by the Triassic magma is also a likely process since the rock exhibit a bimodal age distribution with peaks at 218.8±8.3 Ma and 265.0±2.4 Ma. Hervé *et al.* (2014) reported an age of 255.2±1.8 Ma but these authors discarded two younger single-grain ages at *ca.* 215 Ma and 225 Ma. We therefore think that the Late Triassic age is a plausible date for igneous crystallization of the gabbroic rocks, although some crustal material might have been assimilated in the process.

6. Geochemistry

Major and trace elements abundances for the studied volcanic and plutonic rocks are listed in Table 2 and in Salazar *et al.* (2013). Prior to the description of the geochemical results, the issue of the secondary alteration processes that affected the studied rocks is addressed.

6.1. Alteration

Secondary minerals are very common in the studied samples (see Table 1 and Appendix 1). The alteration minerals in the volcanic rocks can be up to the 25% of the total volume of the rock, whereas in the plutonic rocks is generally less than the 10%, with some exceptions up to 40% (Algodones granites). The exception are: sample CPV-12-105 (Llano de Chocolate beds), a silicified rhyolite or rhyolitic tuff for which the recognized volume of secondary quartz reaches the 85%; sample CPV-12-38 (San Félix Formation), a lithic tuff with a total volume of alteration minerals, mainly secondary quartz, of 39%; four samples of Coastal Cordillera intrusives (CPV-12-91A, CPV-12-92, CPV-12-93 and CPV-12-03) with total volume of alteration minerals ranging from 26 to 12%, being chlorite the main secondary phase; and four samples of the Chollay Plutonic Complex (CT-164q, CT-173q, CT-184q, CT-191q) with total volume of alteration minerals ranging from 26 to 12%, being sericite the main secondary phase. In addition, three samples of pyroclastic rocks (sample CPV-12-38 and CPV-12-49b, San Félix Formation;

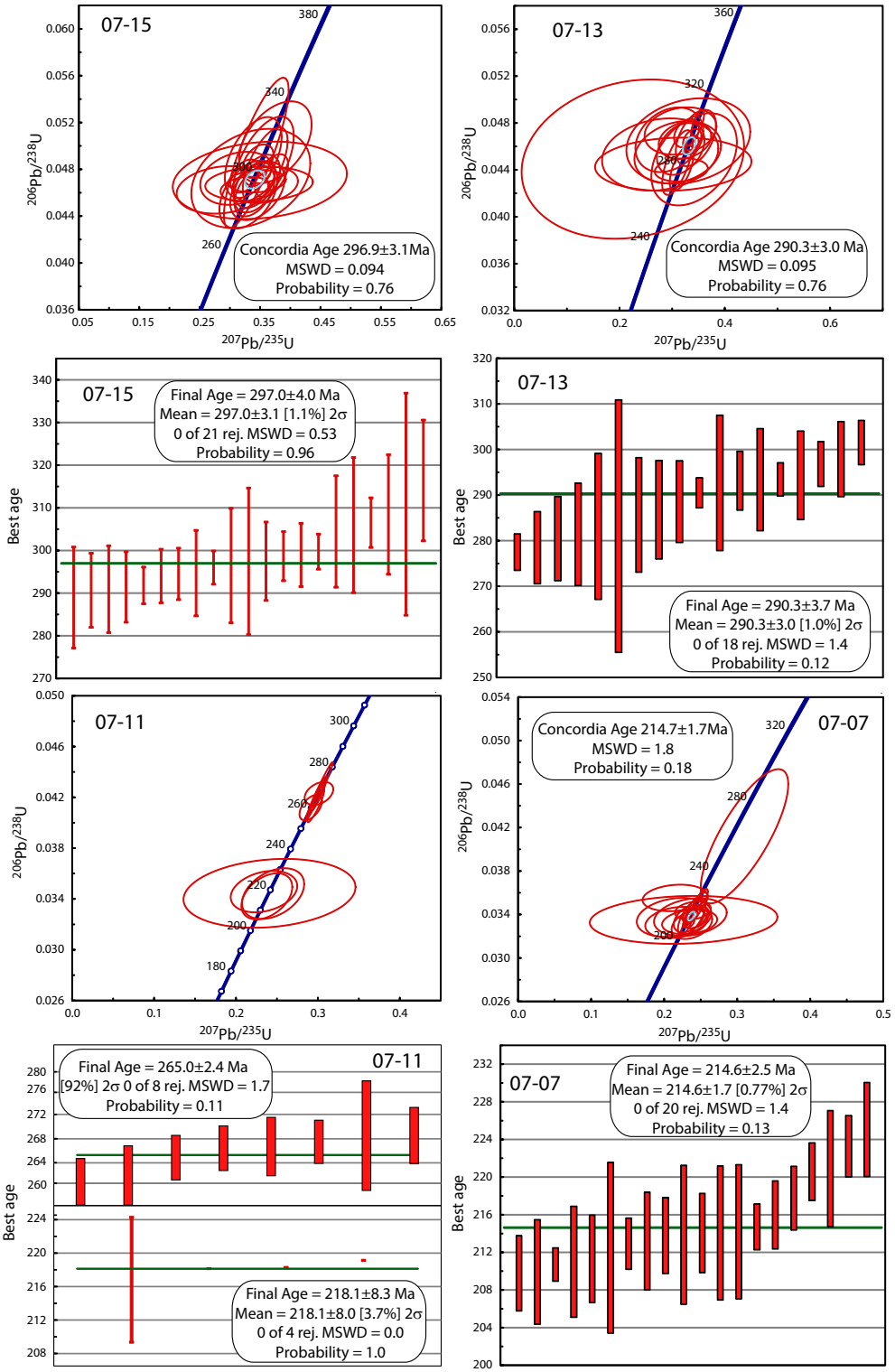

FIG. 3. Tera-Wasserburg concordia and estimated best U-Pb age plots for analyzed samples belonging to the Guanta Unit (O7-15), the Los Tilos Pluton (O7-13), the La Laguna Gabbro (O7-11) and the Montegrande Granite (O7-07).

TABLE 2. XRF AND ICP-MS GEOCHEMICAL DATA FOR THE ANALYZED SAMPLES.

Sample	CPV-12-105	CPV-12-12	CPV-12-127	O7-15	O7-10	O7-11	SCL-02q
Unit	Llano de Chocolate Beds	Llano de Chocolate Beds	Llano de Chocolate Beds	Guanta Unit	La Laguna Gabbro	La Laguna Gabbro	Chollay Plutonic Complex
Lithology	Rhyolite	Dacite	Tuff rhyolitic	Tonalite	Gabbro	Gabbro	Monzogranite
UTM East	286,402	289,084	287,052	366,163	396,451	396,266	410,948
UTM North	6,789,103	6,794,562	6,792,338	6,697,056	6,669,570	6,669,913	6,804,964
SiO_2 %	67.42	72.24	68.71	56.25	47.44	46.25	77.72
TiO_2	<0.01	0.16	0.28	0.75	1.48	1.25	0.09
Al_2O_3	9.50	9.87	12.41	13.33	17.08	17.30	11.89
Fe_2O_3	0.00	0.77	0.65	0.83	0.95	1.04	0.19
FeO	0.00	1.53	1.31	5.55	6.35	6.92	0.38
MnO	0.04	0.06	0.04	0.09	0.08	0.08	0.05
MgO	0.18	0.53	0.58	3.24	4.21	4.72	0.08
CaO	0.31	1.13	1.23	5.57	10.70	9.59	0.27
Na_2O	3.96	2.10	2.35	2.66	2.72	2.51	3.92
K_2O	4.61	3.53	3.91	2.06	1.00	1.40	3.94
P_2O_5	0.02	0.05	0.06	0.19	0.63	0.89	0.02
LOI	12.79	7.98	8.45	7.34	7.78	8.06	0.40
Total %	98.82	99.96	99.98	97.87	100.43	100.01	98.95
La ppm	4.3	38.0	38.6	8.4	27.2	26.3	13.3
Ce	6.9	66.7	67.6	31.9	56.0	53.5	25.5
Pr	1.4	6.1	11.1	3.2	7.2	5.1	2.9
Nd	8.0	29.8	28.1	18.0	31.4	28.4	10.0
Sm	1.8	6.1	5.5	4.3	7.0	6.0	1.9
Eu	0.4	1.3	1.0	1.0	2.4	1.7	0.3
Gd	1.9	5.8	5.1	4.3	6.7	5.7	1.6
Tb	0.3	0.9	0.9	0.7	1.0	0.8	0.3
Dy	1.8	5.2	4.7	4.1	5.6	4.6	2.1
Ho	0.4	1.1	1.0	0.8	1.1	0.9	0.5
Er	1.0	3.2	3.1	2.4	3.0	2.5	1.3
Tm	0.1	0.5	0.5	0.3	0.4	0.3	0.2
Yb	0.9	3.2	3.4	2.2	2.6	2.1	1.6
Lu	0.1	0.5	0.5	0.3	0.4	0.3	0.2
Y	7.6	20.0	18.5	18.8	29.4	14.8	14.1
Sc	1.6	5.5	6.4	13.0	18.8	12.7	2.0
Hf	1.2	2.8	3.3	0.6	5.1	3.0	2.2
Nb	4.1	9.8	9.9	7.6	8.1	6.4	9.5
Ta	0.3	0.7	0.9	0.5	0.4	0.4	1.0
Th	5.1	13.7	27.7	4.2	6.0	6.4	8.6
Zn	117.8	583.1	20.1	59.7	82.4	74.4	<30
Co	0.4	3.5	3.3	17.9	44.3	25.7	<1
Ni	8.0	3.0	2.1	24.3	37.9	33.4	<20
Ba	299.8	2,075.6	624.0	377.2	427.9	431.0	677.0
Cr	53.1	15.2	6.9	18.8	18.8	22.4	<20
V	11.1	2.6	27.2	28.7	12.0	10.2	75.0
Se	0.0	0.0	0.0	0.0	0.0	0.0	0.0
Br	0.0	0.0	0.0	0.0	0.0	0.0	0.0
Cu	15.3	3.6	4.3	8.8	52.8	60.4	10.0
Sr	44.7	167.1	67.1	236.3	530.8	420.2	42.0
Zr	21.9	72.5	85.2	5.9	219.2	118.2	61.0
Rb	38.8	153.3	177.1	54.7	19.2	26.2	138.0
As	0.0	0.0	0.0	0.0	0.0	0.0	<5
Be	0.0	0.0	0.0	0.0	0.0	0.0	3.0
Sb	2.1	0.5	1.2	0.1	0.9	0.3	0.4
Sn	2.3	6.1	7.9	4.5	3.6	3.8	1.0
U	1.6	2.6	3.2	1.7	1.8	1.8	2.3
W	1.8	2.3	2.5	5.4	0.8	0.7	1.2
Bi	0.0	0.0	0.0	0.0	0.0	0.0	<0.1
Cd	0.1	0.1	0.0	0.0	0.0	0.0	0.0
Cs	1.6	2.3	14.6	2.0	3.1	2.5	2.0
Ga	6.9	33.1	17.4	18.4	27.4	20.0	13.0
Ge	0.1	0.4	0.4	0.9	1.3	1.1	2.8
In	0.0	0.0	0.0	0.0	0.0	0.0	<0.1
Mo	0.9	0.1	0.2	1.2	0.5	0.4	<2
Pb	61.5	4.1	12.2	15.9	11.9	10.3	9.0
Ag	0.0	0.0	0.0	0.0	0.0	0.0	1.2
Tl	0.0	0.0	0.0	0.0	0.0	0.0	0.7

Table 2 continued.

Sample	SCL-09q	CPV-12-38*	CPV-12-49b*	CPV-12-23	CPV-12-24	CPV-12-60	SCL-26q*
Unit	Chollay Plutonic Complex	San Félix Formation	San Félix Formation	La Totora Formation	La Totora Formation	La Totora Formation	La Totora Formation
Lithology	Tonalite	Tuff lithic	Tuff lithic	Andesite	Andesite	Basalt	Tuff
UTM East	410.315	362.530	359.174	376.484	383.333	382.348	414.172
UTM North	6.794.865	6.778.657	6.805.415	6.814.323	6.826.718	6.827.655	6.808.064
SiO_2 %	68.47	86.59	72.23	56.61	43.06	44.81	81.32
TiO_2	0.46	0.17	0.14	1.34	1.58	1.10	0.11
Al_2O_3	14.55	5.40	13.20	14.61	16.33	15.21	9.93
Fe_2O_3	1.02	0.00	0.25	1.61	1.81	1.43	0.40
FeO	2.54	0.00	0.50	5.38	9.05	7.16	0.79
MnO	0.07	0.02	0.03	0.11	0.19	0.14	0.01
MgO	1.43	0.12	0.62	2.17	9.09	8.96	0.15
CaO	3.46	0.13	0.27	5.57	7.50	8.86	0.57
Na_2O	3.59	0.31	1.86	3.55	3.77	4.82	1.69
K_2O	2.92	1.95	3.50	1.30	0.08	0.29	3.76
P_2O_5	0.10	0.00	0.03	0.43	0.37	0.33	0.01
LOI	1.16	5.18	7.34	7.31	7.17	6.81	1.94
Total %	99.78	99.87	99.99	99.99	99.99	99.92	100.69
La ppm	23.7	8.9	37.8	26.1	1.3	8.9	31.2
Ce	44.3	31.0	73.4	52.8	6.3	28.5	62.8
Pr	5.0	2.8	12.0	5.1	0.8	3.7	7.2
Nd	18.1	13.7	32.6	28.4	5.0	17.7	26.8
Sm	3.4	3.0	7.0	6.2	1.4	3.6	4.8
Eu	0.8	0.6	1.4	2.0	0.5	1.1	0.3
Gd	2.7	3.3	6.8	6.3	1.4	3.3	3.6
Tb	0.5	0.6	1.1	1.0	0.2	0.5	0.7
Dy	2.6	3.2	6.7	5.6	1.3	2.3	4.2
Ho	0.5	0.6	1.3	1.1	0.3	0.4	0.9
Er	1.7	1.6	3.9	3.2	0.7	1.6	2.6
Tm	0.3	0.2	0.5	0.4	0.1	0.1	0.4
Yb	1.6	1.4	3.6	2.8	0.6	1.0	3.1
Lu	0.3	0.2	0.5	0.4	0.1	0.1	0.4
Y	15.8	12.1	42.8	33.3	2.5	13.3	24.5
Sc	9.0	2.1	4.8	12.0	6.2	20.5	3.0
Hf	4.8	1.1	4.8	6.0	2.7	1.9	4.5
Nb	6.7	6.6	15.6	9.3	3.7	4.8	11.9
Ta	0.6	0.3	0.9	0.5	0.2	0.2	0.9
Th	8.7	5.9	27.2	3.1	0.3	2.0	14.6
Zn	50.0	9.4	20.1	92.9	101.6	114.6	< 30
Co	7.0	2.1	1.1	16.1	43.4	35.1	< 1
Ni	< 20	3.7	6.7	5.1	102.1	153.7	< 20
Ba	794.0	467.8	1662.7	391.7	17.8	43.4	471.0
Cr	< 20	16.4	17.2	5.7	103.8	550.8	< 20
V	157.0	15.0	7.5	4.9	203.8	120.6	6.0
Se	0.0	0.0	0.0	0.0	0.0	0.0	0.0
Br	0.0	0.0	0.0	0.0	0.0	0.0	0.0
Cu	30.0	3.0	2.2	18.1	769.8	7.8	< 10
Sr	249.0	6.6	151.0	444.2	146.5	199.2	41.0
Zr	189.0	19.8	98.8	280.7	127.8	78.9	127.0
Rb	111.0	105.1	136.8	20.8	0.1	3.2	105.0
As	< 5	0.0	0.0	0.0	0.0	0.0	< 5
Be	2.0	0.0	0.0	0.0	0.0	0.0	2.0
Sb	0.3	13.3	0.3	0.0	0.2	0.1	0.4
Sn	2.0	4.3	8.9	3.9	2.5	1.1	4.0
U	1.6	1.1	3.7	0.7	0.2	0.1	2.2
W	2.3	1.8	1.6	0.3	0.2	0.1	1.5
Bi	< 0.1	0.0	0.0	0.0	0.0	0.0	< 0.1
Cd	0.0	0.0	0.0	0.0	0.0	0.0	0.0
Cs	2.7	21.1	2.7	0.5	0.0	0.8	2.3
Ga	16.0	14.3	33.8	20.5	13.7	16.3	11.0
Ge	2.5	0.1	0.3	1.0	1.8	1.2	1.4
In	< 0.1	0.0	0.0	0.0	0.0	0.0	< 0.1
Mo	< 2	0.2	0.4	0.9	0.3	0.3	< 2
Pb	13.0	2.5	12.9	8.9	10.4	9.3	17.0
Ag	2.0	0.0	0.0	0.0	0.0	0.0	2.2
Tl	0.7	0.0	0.0	0.0	0.0	0.0	1.0

Table 2 continued.

Sample	O7-13	O7-07	O7-06	CPV-12-91A	CPV-12-91B	CPV-12-93	CPV-12-92
Unit	Los Tilos	Monte Grande Unit	Monte Grande Unit	Carrizal Bajo Plutonic Complex	Carrizal Bajo Plutonic Complex	Carrizal Bajo Plutonic Complex	Algodones Granite
Lithology	Granite (two mica)	Granite	Granite	Diorite	Tonalite	Granodiorite	Diorite
UTM East	368.473	361.047	357.424	301.526	301.526	288.859	298.038
UTM North	6.695.942	6.666.761	6.668.630	6.884.546	6.884.546	6.878.634	6.887.501
SiO_2 %	67.80	67.42	74.31	51.74	68.22	67.83	53.61
TiO_2	0.08	b.d.l.	0.08	1.33	0.41	0.12	0.91
Al_2O_3	12.71	9.50	9.53	12.62	8.73	10.44	13.59
Fe_2O_3	0.35	0.15	b.d.l.	1.56	1.04	0.37	1.73
FeO	1.15	1.02	b.d.l.	7.79	2.09	0.74	5.76
MnO	0.06	0.04	0.03	0.11	0.05	0.04	0.10
MgO	0.52	0.18	0.20	4.23	0.52	0.33	4.36
CaO	1.85	0.31	0.61	7.32	2.20	1.01	6.21
Na_2O	3.41	3.96	2.76	2.88	2.70	3.63	3.18
K_2O	1.91	4.61	4.70	1.44	1.25	3.96	1.58
P_2O_5	0.07	0.02	b.d.l.	0.50	0.11	0.07	0.26
LOI	9.44	8.03	8.93	8.44	12.54	11.12	8.62
Total %	99.36	95.24	101.14	99.96	99.87	99.65	99.90
La ppm	25.9	45.5	5.2	11.3	57.1	11.5	9.8
Ce	44.1	86.6	7.2	42.4	106.6	38.9	36.1
Pr	4.6	12.1	0.9	4.9	16.6	3.2	3.6
Nd	16.7	38.4	3.9	24.0	45.1	15.7	19.7
Sm	2.8	8.2	0.6	6.1	8.5	3.9	4.5
Eu	0.9	0.9	1.4	1.6	1.5	0.5	1.1
Gd	2.4	7.5	0.5	6.6	7.9	4.2	4.2
Tb	0.3	1.1	0.1	1.2	1.1	0.8	0.6
Dy	1.3	6.1	0.3	7.0	5.2	4.7	3.6
Ho	0.2	1.2	0.1	1.4	1.0	1.0	0.7
Er	0.6	3.4	0.2	4.2	2.8	3.0	2.0
Tm	0.1	0.5	0.0	0.6	0.4	0.5	0.3
Yb	0.5	3.2	0.2	3.9	2.4	3.3	1.8
Lu	0.1	0.5	0.0	0.6	0.4	0.5	0.3
Y	4.3	25.8	1.1	43.0	26.0	33.6	12.3
Sc	2.1	1.9	2.0	17.4	3.8	2.6	10.9
Hf	0.3	0.9	0.3	1.3	2.8	2.4	0.7
Nb	6.6	8.5	7.5	14.3	6.1	6.8	4.0
Ta	0.4	0.4	0.4	0.8	0.3	0.6	0.3
Th	3.2	3.4	2.1	7.7	55.8	14.4	4.2
Zn	55.6	72.0	16.2	67.9	22.2	31.6	61.9
Co	1.9	0.2	0.5	23.8	3.4	2.4	21.1
Ni	3.2	1.3	2.7	31.2	3.6	3.9	30.3
Ba	598.5	505.0	1561.6	233.0	432.9	231.4	214.0
Cr	112.1	4.7	88.9	74.1	5.8	5.5	68.4
V	2.9	1.2	1.0	182.8	22.6	7.1	178.4
Se	0.0	0.0	0.0	0.0	0.0	0.0	0.0
Br	0.0	0.0	0.0	0.0	0.0	0.0	0.0
Cu	3.2	1.2	3.1	24.4	36.6	2.7	44.9
Sr	335.9	8.8	101.1	206.6	130.3	50.0	318.9
Zr	3.7	8.0	6.1	25.6	102.1	74.7	7.3
Rb	30.3	37.7	121.0	33.1	27.6	234.2	18.2
As	0.0	0.0	0.0	0.0	0.0	0.0	0.0
Be	0.0	0.0	0.0	0.0	0.0	0.0	0.0
Sb	0.1	0.1	0.0	0.3	0.2	0.0	0.1
Sn	1.9	3.4	1.1	3.9	5.6	10.3	3.0
U	0.4	0.7	0.3	1.6	1.7	3.8	0.7
W	0.2	0.2	0.4	0.8	0.5	0.2	0.4
Bi	0.0	0.0	0.0	0.0	0.0	0.0	0.0
Cd	0.0	0.0	0.0	0.0	0.0	0.0	0.0
Cs	1.3	0.9	1.4	0.6	0.9	8.2	0.3
Ga	20.1	21.8	27.4	17.3	17.7	15.2	14.8
Ge	0.4	0.4	0.1	1.1	0.5	0.3	0.8
In	0.0	0.0	0.0	0.0	0.0	0.0	0.0
Mo	0.3	0.6	0.1	0.4	0.5	0.4	0.3
Pb	15.6	15.4	29.8	8.5	14.9	20.5	5.5
Ag	0.0	0.0	0.0	0.0	0.0	0.0	0.0
Tl	0.0	0.0	0.0	0.0	0.0	0.0	0.0

* Strongly altered volcaniclastic samples, with minor lithic content.

SCL-26q, La Totora Formation) are strongly altered and lithic fragments were not separate, which implies that these samples have not been considered in the interpretation of the tectonic implications. Calcite and sericite are ubiquitous alteration mineral phases in the volcanic rocks, whereas clay minerals, chlorite and sericite are the dominant secondary minerals in the plutonic rocks. Sericite and clay minerals replace plagioclase phenocrysts and calcite occurs in fractures, amygdules or as replacement of phenocrysts. The high loss on ignition in some of the volcanic and plutonic rocks is consistent with the widespread occurrence of calcite (Table 2).

Given that the discrimination of the convergent margin and within plate tectonic settings for igneous rocks is largely based in the content of incompatible (alkaline, large radii lithophile and high field strength) elements of the analyzed samples, and taking into account that some of these elements are mobile in hydrothermal processes, it is necessary to test the extent of mobility for the studied rocks. A comparison between the total alkalis *versus* silica (TAS) and Zr/Ti *versus* Nb/Yb classification diagrams was made (Figs. 4c, 4d). Slight enrichment in alkalis is observed in the volcanic rocks, which plot near the alkaline/sub-alkaline boundary. However, the classification based on the more immobile elements discards the alkaline character of the same rocks, with the exception of sample CPV-12-24, a basalt from the La Totora Formation. The potential bias of some mobile major and trace elements along with the high amount of material loss on ignition, that affects particularly the major elements, imply that the interpretations of the tectonic setting of the magmas that generated the studied rocks must be done with caution and based on the behavior of the less mobile elements, such as the rare earth (REE) and high field strength (HFSE) elements. In this work, we only considered for tectonic implications the rocks with less than 10 % of total volume of alteration minerals.

6.2. Major Elements

The contents of SiO_2 (on anhydrous basis) of the volcanic rocks with variable alteration grade range between 48% and 91% (Fig. 4c). The pyroclastic rocks of the La Totora and San Félix Formations and the Llano de Chocolate Beds that have the highest SiO_2 content are strong altered. This is consistent with the dispersion of the alkalis displayed for these samples in Fig. 4c. Although the number of studied samples precludes a significant statistical approach, a bimodal distribution of the volcanic rock within the different units is not observed, at least for the major element content. The alkali content of the rocks range from 3 to 8 wt% (oxide), and in general it increases with higher SiO_2 content. Exceptions to this pattern are samples CPV-12-38 and CPV-12-105 with 2% and 10% alkalis, respectively. According to their SiO_2 and K_2O content the studied rocks would have calc-alkaline and high-K calc-alkaline affinities (Fig. 4c)(Peccerillo and Taylor, 1976; Irvine and Baragar, 1971) The wt% of TiO_2, MgO and FeO_t vary from 0.08 to 2.20, 0.49 to 16.00 and from 0.30 to 13.50, respectively. The dispersion for these elements is much less than for the alkalis and in general their concentration decreases with increasing SiO_2 content. The Al_2O_3 content ranges between 8.83 and 18.50 wt%, decreasing, first very slightly and then progressively, with increasing SiO_2 content. The systematic decrease in the contents of TiO_2, FeO_t, MgO, Al_2O_3 and CaO is compatible with progressive fractionation of plagioclase, Fe-Ti oxides, olivine and clinopyroxene, which is consistent with the observed mineralogy in the studied rocks (Appendix 1).

6.3. Trace elements

As observed in the multi-element diagrams (Fig. 5) most of the studied samples show enrichment in LILE compared to HFSE, relative to primitive mantle concentrations. High contents of Pb as well as a depletion in Nb-Ta, Ti and P are observed in rocks of all units. The volcanic rocks show a much larger dispersion in LILE than any of the plutonic lithologies, especially Cs and Rb. Such pattern is likely due to hydrothermal alteration or very low grade metamorphism. The rocks of the La Totora Formation have the lowest LILE contents but still enriched in this groups of elements compared to HFSE.

Both plutonic and volcanic units show rather steep chondrite-normalized REE patterns (Fig. 5), with $(La/Yb)_N$ ranging from 3.4 to 52.2 for Permian rocks to 3.1 to 43.4 for Triassic rocks. Eu anomalies in volcanic rocks show a moderately negative correlation to SiO_2 in all units, suggesting a modest contribution of plagioclase fractionation to magma

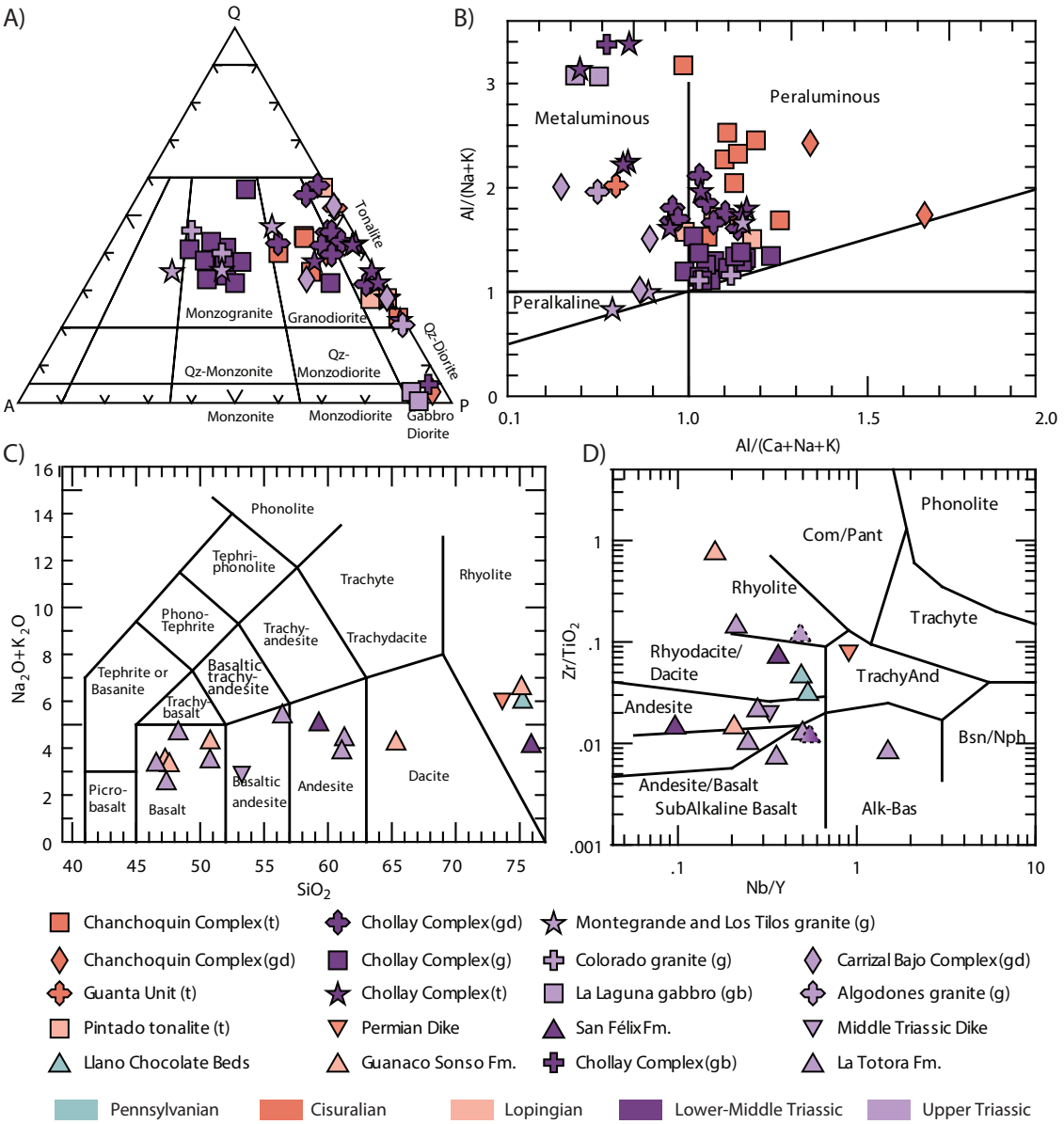

FIG. 4. **A.** QAP classification and **B.** alumina saturation index diagrams for plutonic rocks (Shand, 1927), **C.** TAS (Lebas *et al.,* 1986) and **D.** Nb/Y *versus* Zr/TiO_2 (Winchester and Floyd, 1977) classification diagrams for volcanic rocks. Symbols with dashed lines and color gradient represent the two strongly altered samples of volcaniclastic rocks from the San Félix (CPV-12-38) and La Totora (SCL-26Q) formation.

evolution. The Eu/Eu* ranges from 0.6 to 1.2 in most of the volcanic rocks, and it around 1.0 for the majority of Triassic rocks (Fig.6a), suggesting relatively high oxygen fugacity conditions for those magmas. The plutonic rocks also lack significant negative Eu anomalies but have a wider range of Eu/Eu* between 0.2 and 1.8 (Fig. 7a). The Upper Triassic intrusives, both in the Coastal and Frontal cordilleras, exhibit the most marked negative anomalies and most positive as well, whereas the Chollay complex and the Permian intrusions have Eu/Eu* values around 1.

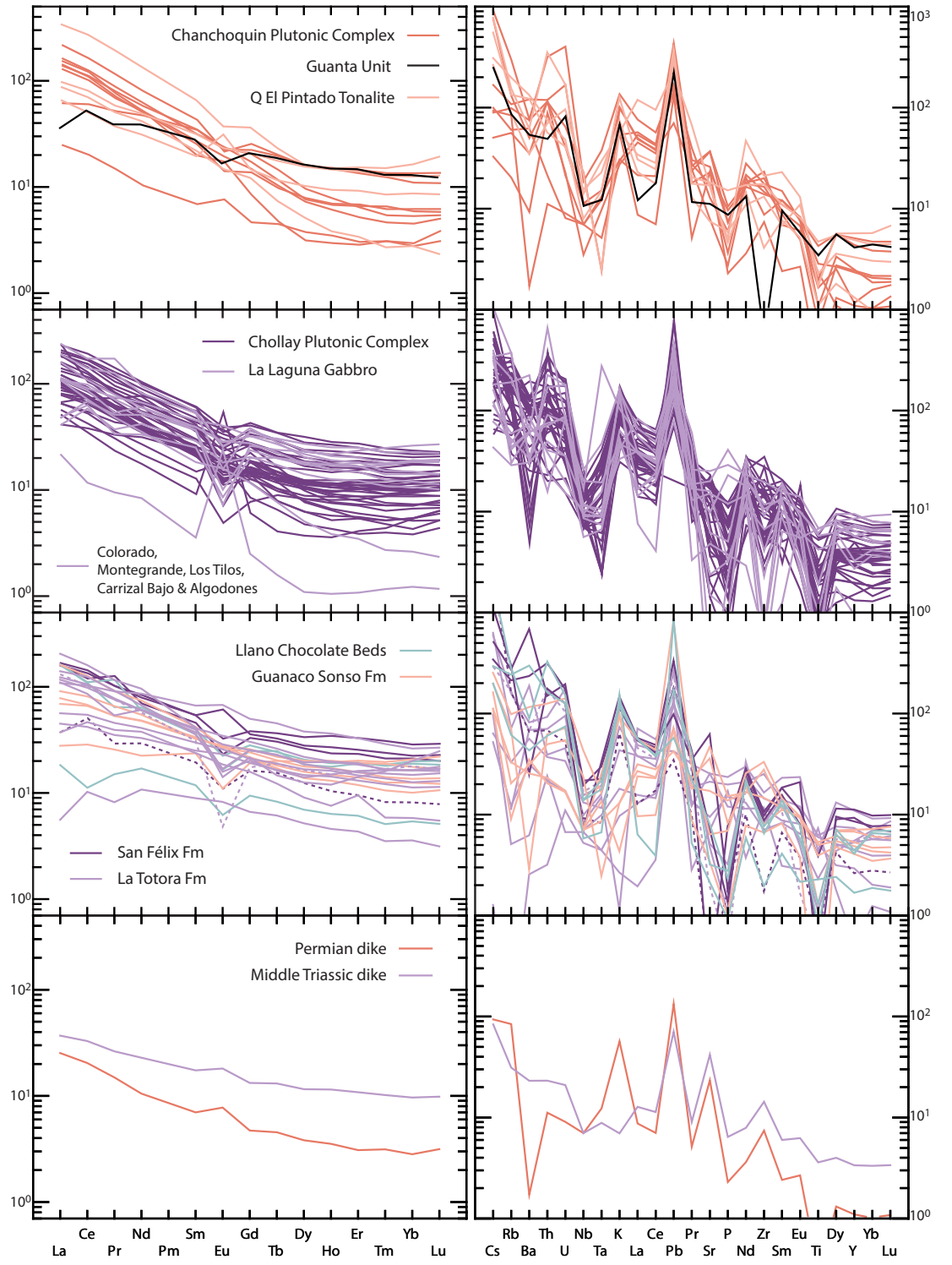

FIG. 5. Spider diagrams of chondrite-normalized rare earth (left) and primitive mantle-normalized (right) trace elements abundance in the studied rocks. Normalizing values are from Sun and McDonough (1989). Dashed lines represent the two strongly altered samples of volcaniclastic rocks from the San Félix (CPV-12-38) and La Totora (SCL-26Q) formation.

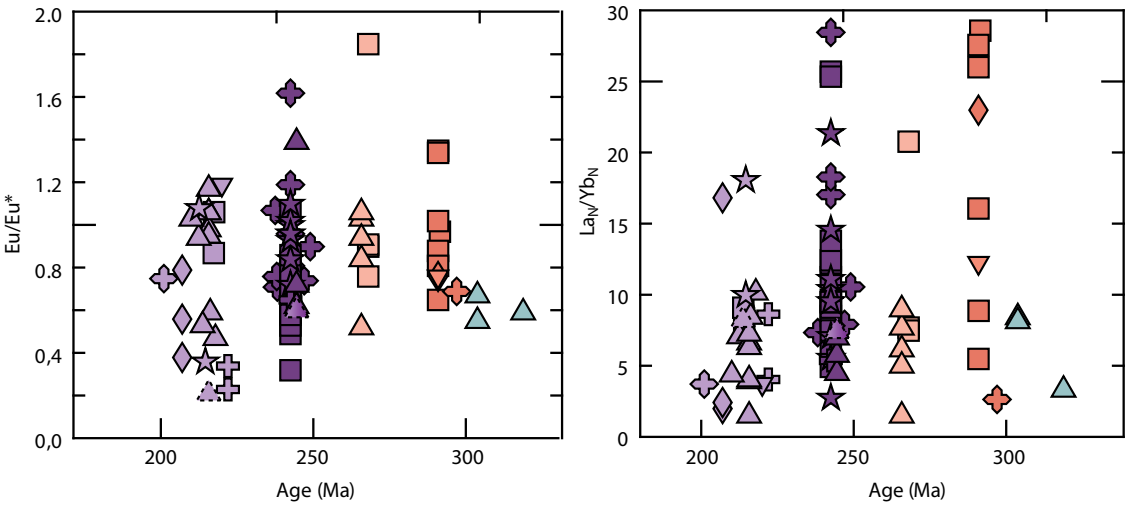

FIG. 6. Age *versus* Eu/Eu* and La_N/Yb_N for the studied samples. All REE values normalized to chondrite abundances (Sun and McDonough, 1989). Symbols with dashed lines and color gradient represent the two strongly altered samples of volcaniclastic rocks from the San Félix (CPV-12-38) and La Totora (SCL-26Q) formation.

7. Discussion

7.1 . Sources and evolution of the proto-Andean magmatism

The studied rocks are very heterogeneous both petrographically and from their major element composition. The trace elements content is also variable, but they display similar geochemical patterns (*e.g.,* REE) suggesting uniform chemical behavior (Fig. 5). In particular, the marked enrichment in LILE over HFSE is present in all the spider diagrams of figure 5, both for plutonic and volcanic rocks. The volcanic rocks are all subalkaline and plot within the calk-alkaline field of the AFM diagram (Fig. 7a). All but one of the basic and intermediate samples (CPV-12-24 of the La Totora Formation) have also HFSE contents representative of calc-alkaline affinities (Fig. 7b) and the more acidic rocks plot in the field of arc granites based on their LILE and HFSE contents (Fig. 7c, e). Although the number of analyzed volcanic rocks does not allow a robust statistical analysis, it is noteworthy to point out that they comprise the entire petrographic range for subalkaline volcanics, from basalt to rhyolites and there is no bimodal distribution in their composition (Fig. 4c, d). The plutonic rocks also lack bimodal distribution of their compositional ranges, and tonalite is the most abundant lithological type, followed by monzogranite and grandiorite (Fig. 4a). Very few basic intrusions, such as gabbro or diorite, are found among the studied intrusive units (Fig. 4a). In the tectonic discrimination diagrams of Pearce *et al.* (1984), nearly all samples plot in the "Volcanic Arc Granite" field (Fig. 7d, f). Only two samples of the Colorado Syenogranite unit are outside this pattern, plotting in the field of "within plate magmatism" (Fig. 7d).

The Colorado Syenogranite, the La Laguna Gabbro and the Montegrande granite are among the intrusive units with alkaline within plate affinity that are described in the literature (Parada, 1981, 1982; 1988; Nasi *et al.,* 1985; Mpodozis and Kay, 1992) as representatives of the Upper Triassic magmatism. Taking into account the Colorado Syenogranite and the La Totora Formation samples analyzed in this study, it is clear that alkaline magmatism did occur during the Upper Triassic in the present-day Frontal Cordillera. Its volume and areal distribution however, seem to be significantly more restricted (Fig. 1) than that of the calc-alkaline magmatism as it was proposed before and it cannot be considered as representative of the main magmatic events or fluxes that built the continental crust during the Triassic. The origin of this alkaline magmatism may be related to the establishment of the arc in the present-day Coastal Cordillera (see below).

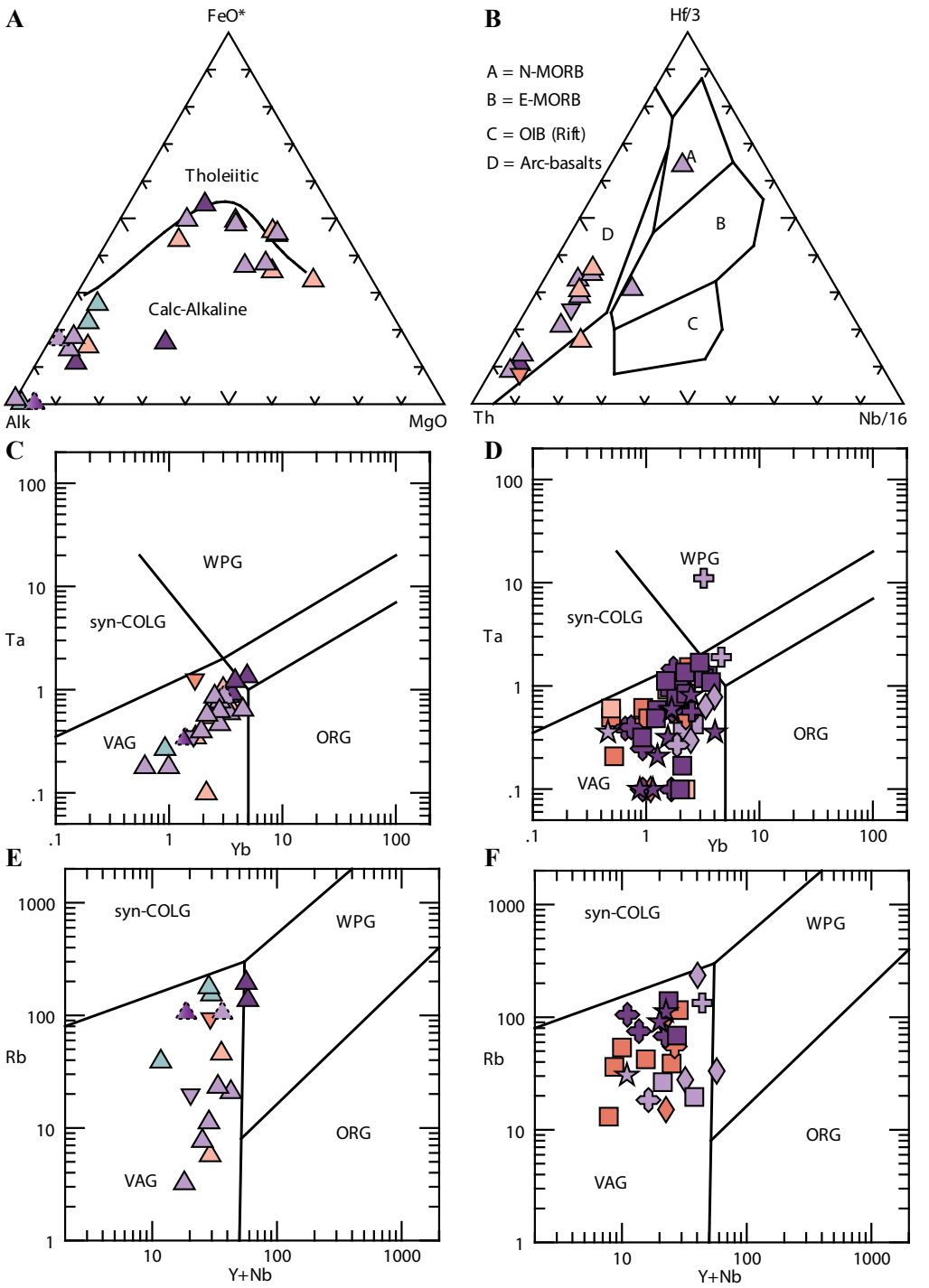

FIG. 7. Tectonic discrimination diagrams for the studied samples. **A.** AFM (Irvine and Baragar, 1971) and **B.** Th-Nb-Hf for basic and intermediated volcanic rocks; Yb *versus* Ta diagram (Pearce *et al.,* 1984) for **C.** acid volcanic and **D.** plutonic rocks; Yb+Nb *versus* Rb (Pearce *et al.,* 1984) for **E.** acid volcanic and **D.** plutonic rocks. Symbols with dashed lines and color gradient represent the two strongly altered samples of volcaniclastic rocks from the San Félix (CPV-12-38) and La Totora (SCL-26Q) formation.

All volcanic rocks are highly porphyritic, suggesting a probably elevated water content of the magmas that favored crystal growth over nucleation prior to volatile inmiscibility or degassing (Cashman and Blundy, 2000; Winter, 2010). The ubiquitous presence of magnetite as the main Fe-Ti oxide mineral phase in both plutonic and volcanic rocks is also an indicator of rather elevated f_{O2} conditions in the magmas (Buddington and Lindsley, 1964). Hydrated minerals such as amphibole and biotite occur in all the petrographic range of the plutonic rocks, from gabbro to syenogranite, which is an undoubtedly evidence that the magmas were hydrated. These petrographic and geochemical patterns are often interpreted as the result of flux-melting of an asthenospheric mantle source, a process that usually takes place at convergent margins were an oceanic plate is subducted under the continent (Stern, 2002 and references therein).

If the magmatic source was indeed a depleted mantle, subsequently metasomatized by fluids that enriched it in mobile elements released by mineral breakdown of hydrated minerals from the subducted slab, then an assimilation of the continental crust during the ascent of such mantle-derived melts is likely (Hildreth and Moorbarth, 1988), especially because the acid components in the plutonic and volcanic rocks are volumetrically dominant. The subduction-related signature is present in both peraluminous and metaluminous intrusives, suggesting that such signal is not only derived from crustal assimilation. Even though high SiO_2, Na_2O, K_2O and REE contents are observed, evidences of fractional crystallization are not entirely coupled to this signal. For example the rocks with the highest REE contents lack the characteristic negative Eu-anomaly associated to fractionation of plagioclase during magma differentiation (Table 2). The degree of crustal assimilation during the Triassic must have been, however, restricted or at least lower than that of the Paleozoic magmatism. This is inferred from the alumina content of the plutonic rocks, which is generally lower for the Chollay and other Triassic intrusives than for the Permian plutons (Fig. 4b). A similar hypothesis has been presented by Hervé *et al.* (2014) and del Rey *et al.* (2016) for the plutonic rocks of the Frontal Cordillera at the same latitudes of the present study. Based on the coupled variation between $^{176}Hf/^{177}Hf$ and $d^{18}O$ and the crystallization age of zircons from these units, these authors concluded that the crustal contamination of the magma sources decreased steadily from the Carboniferous to the Triassic. This is in agreement with the regional extension that should have taken place at continental margin as it has been proposed by several authors (Nasi *et al.,* 1985; Mpodozis and Ramos, 1989; Mpodozis and Kay, 1992) and can also be related to crustal thinning since La_N/Yb_N for Triassic rocks are lower than their Permian counterparts (Fig. 6b). The decrease of a crustal component in the magma sources during the Triassic therefore suggest that the geochemical signature of the studied rocks cannot be solely attributed to heritage from partial melting of a crustal protolith formed during the Gondwana orogeny or earlier.

7.2. Tectonic framework for the Triassic magmatism: passive or active continental margin?

Current models for the tectonic setting of the South American margin during the Triassic, propose that subduction ceased or it was significantly diminished due to global extensional forces operating on the tectonic plates at this time (Mpodozis and Ramos, 1989) or morphed into a soft collision due to accretion of an allochtonous terrain to the continental margin (Mpodozis and Kay, 1992). Evidences supporting these models come both from field geology and geochemistry of Permian to Triassic rocks cropping out in Chile and Argentina. However, in light of the recently updated geological cartography and the more robust geochemical databases for relevant units, alternative tectonic setting cannot be ruled out (Del Rey *et al.,* 2016).

The lines of evidence for the extensional-setting model in present-day Argentinean territory are in summary: **a.** the existence of huge volume of acid magmatism genetically related to crustal anatexis, represented by the Choiyoi group, a unit that is located along the eastern flank of the Andes, between 20° and 40°S (Llambías and Sato, 1990, 1995; Llambías *et al.,* 1993, 2003); **b.** the generation of basaltic flows of alkaline or within plate geochemical signature, genetically related to the last stage of the Choiyoi Group magmatism (Ramos and Kay, 1991), **c.** the sedimentological and structural framework of rift activity in the Cuyo and Ichigualasto basins, both of Lower to Upper Triassic age (Spalletti, 1997; Spalletti *et al.,* 2006; Giambiagi and Martínez, 2008; Giambiagi

et al., 2011) and d) the petrological, sedimentological and structural framework of rift, and subduction-related, activity for the Uppermost Triassic-Lower Jurassic Pre-Cuyo group of the Neuquén Basin in Argentina (Spalletti, 1997; Franzese and Spalletti, 2001; Bechis *et al.,* 2010; D'Elia *et al.,* 2012a, b).

Along the western flank of the Andes and the forearc region of northern Chile between 28 and 31º S, however, the magmatic units that can be related to rift activity are scarce. Bimodal magmatism with crustal or intraplate signature has been reported in the Middle to Upper Triassic Pichidangui Formation (Morata *et al.,* 2000) and in the Limarí Complex (Parada *et al.,* 1991, 1999) at the Coastal Cordillera of north central Chile; and bimodal intrusions of Upper Triassic age had long been recognized in the Frontal Cordillera (~29-30º S) (Parada, 1982, 1988; Nasi *et al.,* 1985; Mpodozis and Kay, 1992; Hervé *et al.,* 2014). In both cases, the volume of magmatism is restricted to the total volume of volcanism and plutonism of the Triassic period (see Fig. 1). Some of the Permian to Lower Triassic volcanic units that are considered to be equivalent to the Choiyoi Group (La Tabla, Pantanoso and Guanaco Sonso/Pastos Blancos formations) do not exhibit geochemical features of extensive crustal contribution, furthermore, the available isotopic data from the literature, would favor the hypothesis of mixed magma sources, a depleted mantle and the continental crust (Parada, 2013; Hervé *et al.,* 2014; Del Rey *et al.,* 2016). Alkaline and/or tholeiitic basalts associated to the late stages of this acid magmatism, and commonly interpreted as dry primitive volcanism resulting from low degrees of decompression melting of the ascending asthenospheric mantle in a rift context, is not found. Basaltic and basaltic-andesitic flows that could correspond to rift activity are described in units such as the La Totora, La Ternera and Quebrada del Salitre Formation in the Precordillera and Frontal cordillera between 27º and 30º S, but they lack alkaline geochemical signature and their age is constrained to the Late Triassic (Reutter, 1974; Ribba *et al.,* 1988; Blanco, 1996; Cornejo and Mpodozis, 1997), more than 20 Ma after ceasing of the Choiyoi-related acid volcanism (Llambías *et al.,* 1993). Recent works have reported Triassic ages for some of the accretionary prisms in northernmost Chile (Casquet *et al.,* 2014), suggesting that generation of an accretionary wedge as the result of subduction of an oceanic plate at the continental margin was an ongoing process at least until the Triassic and did not stop prior to the Carboniferous as it has been proposed before (Parada *et al.,* 1999)

The differences in the magmatic products at both sides of the Andean range are thus important and call for likely distinct patterns of lithospheric evolution during the Triassic. In the continental interior, stretching of the lithosphere induced crustal anatexis due to ascent of the asthenospheric mantle generating well developed NW-oriented depocenters that accommodated the rift deformation (Spalletti, 1997; Llambías *et al.,* 2003; Giambiagi *et al.,* 2011). The geochemical and petrological characteristics of the volcanic and plutonic rocks studied in this paper strongly suggest that they were generated in a subduction setting and the subduction was a continuous process that generated most of the magmatism in the arc region (Fig. 8a).

7.3. Permian to Triassic margin architecture in the studied segment

Even though evidences supporting the idea that continental margin was subjected to active subduction of an oceanic plate during the Triassic have been collected from petrology and geochemistry, the architecture of the supra-subduction zone is still undetermined. The Llano de Chocolate beds have been interpreted as forearc magmatism occurred during the Permian because of their location close to the coeval accretionary prism (Creixell *et al.,* 2016). Given the texture and composition of the Chanchoquin and Chollay plutonic complexes (coarse grained, mainly granodioritic to tonalitic, biotite and hornblende-bearing intrusives), they can be interpreted as representative of the root of an active continental magmatic arc developed from the Permian to the Middle Triassic (Pitcher *et al.,* 1985; Pitcher, 1993; Winter, 2010). The Triassic Guanaco Sonso and Pastos Blancos formations would then represent shallower parts of the arc region, and the San Félix Formation would represent a proximal forearc basin that was active at least until the Early Triassic. Both units are composed of rhyolithic volcanic rocks similar in texture and composition to the subduction-related Miocene to recent acid volcanism emplaced in the same segment of the Andean arc (Kay and Mpodozis, 2001, 2002; Kay *et al.,* 2013).

The La Totora Formation on the other hand, is composed of more undifferentiated volcanics and

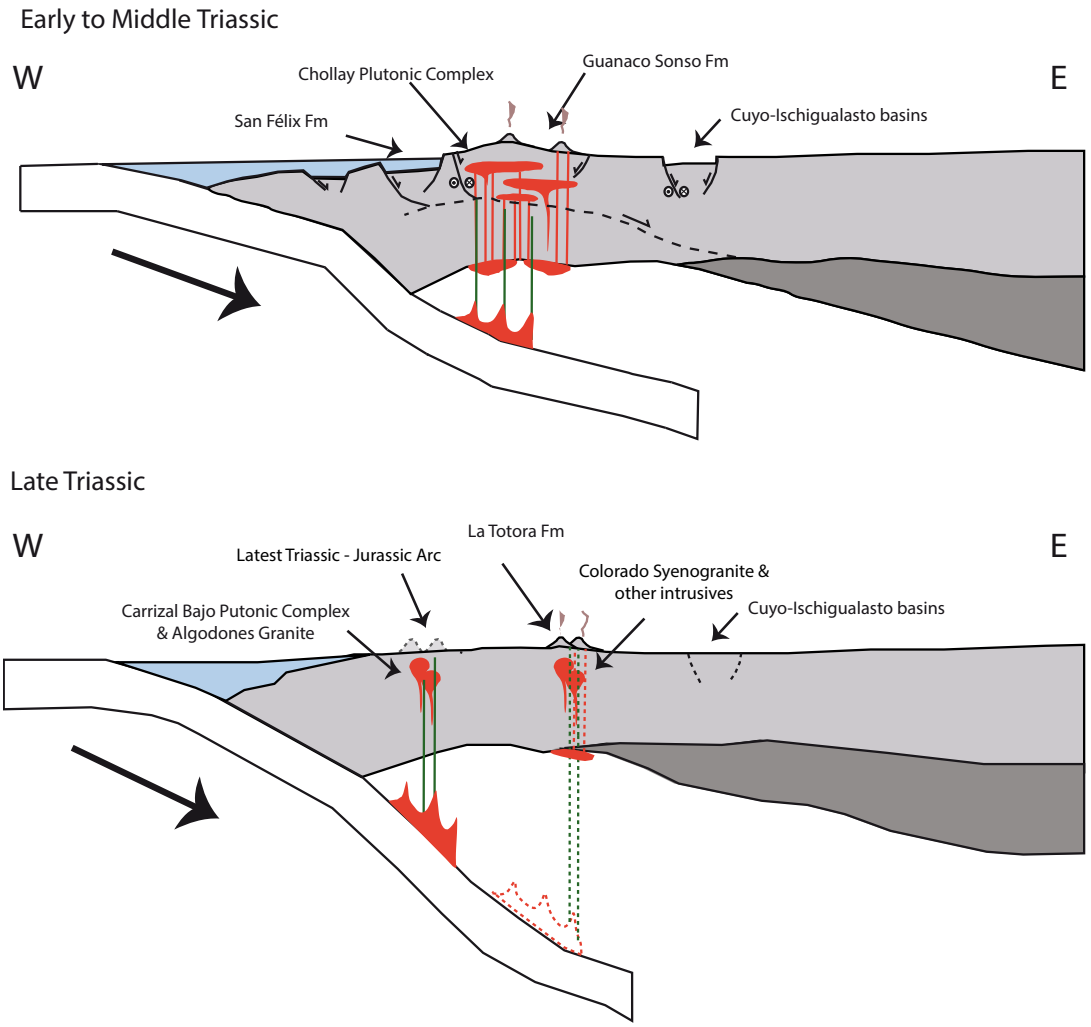

FIG. 8. Proposed tectonic setting for the Triassic magmatism at 28º-30º15' S in the South American margin.

restricted to the Norian-Raethian, although it still retains the subduction-related geochemical and petrological signature. During the Upper Triassic plutonic bodies with alkaline or within plate affinities were intruded (La Laguna Gabbro, Colorado Syenogranite, Montegrande granite). The data presented in this study indicate that these units also have the geochemical signature of arc magmas, but along with the La Totora Formation they comprise the time frame prior to the establishment of the arc at the Coastal Cordillera during the Hettangian (Mpodozis and Ramos, 1989; Parada *et al.,* 1999) (Fig. 8b). The first pulses of the well-known early Andean arc are represented by the La Negra Formation and its equivalents (Rogers and Hawkesworth, 1989; Pichowiak *et al.,* 1990; Pichowiak, 1994) but given the signature of the Coastal Cordillera plutonic bodies studied in this work, they may have been the result of the earliest arc activity in the present-day coastal region. Furthermore, recent studies have reported Rhaetian volcanism in the Coastal Cordillera at 20°-22° S (Sepúlveda *et al.,* 2014). Changes in the geometry of the subducted lithosphere or in tectonic conditions of the upper plate may have induced shift in the arc locus from the Frontal Cordillera to the Coastal Cordillera, but the precise timing an origin of such shifting is yet unknown.

8. Concluding remarks

The Triassic magmatism at the present-day Coastal and Frontal Cordilleras between 28°00' and 29°30' S is mainly represented by plutonic units comprising tonalitic to monzogranite rocks, with scarce syenogranites and more basic rocks such as gabbro and diorite, of which the Chollay Plutonic Complex is the volumetrically most important. Volcanic sequences are more restricted but not uncommon, and they are composed of rocks ranging from basalt to rhyolite, being more abundant the differentiated rocks.

The Permian to Jurassic rocks have petrological and geochemical characteristics typical of subduction-related magmas: calc-alkaline or volcanic arc granite affinities, mafic hydrated minerals as major constituent of the rocks, highly porphyritic texture in the volcanics, magnetite as the main Fe-Ti oxide mineral phase, systematic enrichment of LILE versus HFSE when compared to primitive mantle abundances and Nb-Ta troughs. Although alkaline magmatism of within plate affinities is also found, it is significantly more restricted in terms of total volume and areal distribution and unlikely to be representative of the main Triassic magmatic events.

The detailed architecture of the Andean margin from the Permian to the Triassic is relatively unknown. The Chanchoquín and Chollay plutonic complexes would represent the roots of a magmatic arc developed from the Permian to the Middle or early Late Triassic, whereas the Guanaco Sonso and Pastos Blancos formations would be the shallower parts of the volcanic arc. The San Félix formation likely represent a forearc basin developed throughout the Triassic. The La Totora Formation and some intrusive units that may have slight intraplate or transitional geochemical signature are products of a magmatism developed immediately before the establishment of the magmatic arc in the present-day coastal cordillera, which took place at some time during the Rhaetian to Early Jurassic.

Acknowledgements

This research was funded through the Fondecyt grant 1120715 and the Plan Nacional de Geología of the Servicio Nacional de Geología y Minería (SERNAGEOMIN). M. Ortiz, R. Merino and I. Murillo are thanked for the fruitful discussions on the updated geological mapping in northern Chile. The review of S. Kay greatly improved an earlier version of this manuscript.

References

Arévalo, C.; Welkner, D. 2008. Geología del área Carrizal Bajo-Chacritas, Región de Atacama. Servicio Nacional de Geología y Minería, Carta Geológica de Chile, Serie Geología Básica 111: 67 p., 1 mapa 1:100.000.

Bechis, F.; Giambiagi, L.; García, V.; Lanés, S.; Cristallini, E.; Tunik, M. 2010. Kinematic analysis of a transtensional fault system: The Atuel depocenter of the Neuquén basin, southern Central Andes, Argentina. Journal of Structural Geology 32: 886-899. doi: 10.1016/j.jsg.2010.03.009.

Blanco, N. 1996. Sedimentología y ambientes depositacionales de la Formación La Ternera, Triásico Superior de la Precordillera Andina de Copiapó, Región de Atacama, Chile, Memoria de Título (Inédito), Universidad de Concepción: 250 p. Concepción.

Brook, M.; Pankhurst, R.; Sheperd, G.; Spiro, T. 1987. Andcrhon: Andean geochronology and metallogenesis. British Geological Survey, Overseas Development Administration (unpublished open file report): 137 p. London.

Buddington, A.F.; Lindsley, D.H. 1964. Iron-titanium oxide minerals and synthetic equivalents. Journal of Petrology 54: 310-357.

Cashman, K.; Blundy, J. 2000. Degassing and crystallization of ascending andesite and dacite. Philosophical Transactions of the Royal Society of London Series A, 358 (1770): 1487-1513.

Casquet, C.; Hervé, F.; Pankhurst, R.J.; Baldo, E.; Calderón, M.; Fanning, C.M.; Rapela, C.W.; Dahlquist, J. 2014. The Mejillonia suspect terrane (Northern Chile): Late Triassic fast burial and metamorphism of sediments in a magmatic arc environment extending into the Early Jurassic. Gondwana Research 25: 1272-1286.

Chapman, A.D.; Ducea, M.N.; McQuarrie, N.; Coble, M.; Petrescu, L.; Hoffman, D. 2015, Constraints on plateau architecture and assembly from deep crustal xenoliths, northern Altiplano (SE Perú). Geological Society of America Bulletin 127: 1777-1797.

Cornejo, P.; Mpodozis, C. 1997. El rift Triásico-Sinemuriano de Sierra Exploradora, Cordillera de Domeyko (25°-26°): asociaciones de facies y reconstrucción tectónica. *In* Congreso Geológico Chileno, No. 8, Actas 1: 550-554. Antofagasta.

Creixell, C.; Parada, M.A.; Morata, D.; Roperch, P.; Arriagada, C. 2009. The genetic relationship between mafic dike swarms and plutonic reservoirs in the Mesozoic of central Chile (30°33°45' S): Insights from AMS and geochemistry. International Journal of Earth Sciences 98: 177-201.

Creixell, C.; Ortiz, M.; Arévalo, C. 2012. Geología del área Carrizalillo-El Tofo, Regiones de Atacama y Coquimbo. Servicio Nacional de Geología y Minería, Carta Geológica de Chile, Serie Geología Básica 133-134: 82 p., 1 mapa 1:100.000.

Creixell:, C.; Labbé, M.; Arévalo, C.; Salazar, E. 2013. Geología del área Estación Chañar-Junta de Chingoles, Regiones de Atacama y Coquimbo. Servicio Nacional de Geología y Minería, Carta Geológica de Chile, Serie Geología Básica 150: 85 p., 1 mapa escala 1:100.000. Santiago.

Creixell, C.; Oliveros, V.; Vásquez, P.; Navarro, J.; Vallejos, D.; Valin, X.; Godoy, E.; Ducea, M.N. 2016. Geodynamics of Late Carboniferous Early Permian forearc in north Chile (28°30-29°30' S). Journal of the Geological Society 173 (5): 757-772. doi:10.1144/jgs2016-010.

Del Rey, A.; Arriagada, C.; Dekart, K.; Martínez, F. 2016. Resolving the paradigm of the late Paleozoic-Triassic Chilean magmatism: Isotopic approach. Gondwana Research 37: 172-181. doi: 10.1016/j.gr.2016.06.008.

D'Elia, L.; Muravchik, M.; Franzese, J.R.; Bilmes, A. 2012a. Volcanismo de sin-rift de la Cuenca Neuquina, Argentina: relación con la evolución Triásico Tardía-Jurásico Temprano del margen Andino. Andean Geology 39 (1): 106-132. doi: 10.5027/andgeoV39N1-a06.

D'Elia, L.; Muravchik, M.; Franzese, J.R.; López, L. 2012b. Tectonostratigraphic analysis of the Late Triassic-Early Jurassic syn-rift sequence of the Neuquen Basin in the Sanico depocentre, Neuquén Province, Argentina. Andean Geology 39 (1): 133-157. doi: 10.5027/andgeoV39N1-a07.

Franzese, J.R.; Spalletti, L.A. 2001. Late-Triassic-Early Jurassic continental extension in southwestern Gondwana: tectonic segmentation and pre-break-up rifting. Journal of South American Earth Sciences 14: 257-270. doi:10.1016/S0895-9811(01)00029-3.

Gehrels, G.E.; Valencia, V.A.; Ruiz, J. 2008. Enhanced precision, accuracy, efficiency, and spatial resolution of U-Pb ages by laser ablation-multicollector-inductively coupled plasma-mass spectometry: Geochemistry Geophysics Geosystems, Q03017. doi: 10.1029/2007GC001805.

Giambiagi, L.; Martínez, A. 2008. Permo-Triassic oblique extension in the Potrerillos-Uspallata area, western Argentina. Journal of South American Earth Sciencies 26: 252-260. doi: 10.1016/j.jsames.2008.08.008.

Giambiagi, L.; Mescua, J.; Bechis, F.; Martínez, A.; Folguera, A. 2011. Pre-Andean deformation of the Precordillera southern sector, southern Central Andes. Geosphere 7: 219-239. doi: 10.1130/GES00572.1.

Godoy, E.; Lara, L. 1998. Hojas Chañaral y Diego de Almagro, Región de Atacama. Servicio Nacional de Geología y Minería, Mapas Geológicos 5-6, 1 mapa escala 1:100.000.

Hervé, F.; Fanning, C.M.; Calderón, M.; Mpodozis, M. 2014. Early Permian to Late Triassic batholiths of the Chilean Frontal Cordillera (28°-31°S): SHRIMP U-Pb zircon ages and Lu-Hf and O isotope systematics. Lithos 184-187: 436-446. doi:10.1016/j.lithos.2013.10.018.

Hildreth, W.; Moorbath, S. 1988. Crustal contributions to arc magmatism in the Andes of Central Chile. Contributions to Mineralogy and Petrology 98: 455-489.

Irvine, T.; Baragar, W. 1971. A guide to the chemical classification of the common volcanic rocks. Canadian Journal of Earth Sciences 8: 523-548.

Kay, S.M.; Mpodozis, C. 2001. Central Andean ore deposits linked to evolving shallow subduction systems and thickening Crust. GSA Today 11: 4-9.

Kay, S.M.; Mpodozis, C. 2002. Andean Adakites: Three Ways to Make Them. Acta Petrologica Sinica 18: 303-311.

Kay, S.M.; Mpodozis, C.; Gardeweg, M. 2013. Magma sources and tectonic setting of Central Andean andesites (25.5-28ºS) related to crustal thickening, forearc subduction erosion and delamination. *In* Orogenic Andesites and Crustal Growth (Gómez-Tuena, A.; Straub, S.M.; Zellmer, G.F.; editors). Geological Society, Special Publication 385: 303-334. London.

Lebas, M.J.; Lemaitre, R.W.; Streckeisen, A.; Zanettin, B. 1986. A Chemical Classification of Volcanic-Rocks Based on the Total Alkali Silica Diagram. Journal of Petrology 27: 745-750.

Llambías, E.J.; Sato, A.M. 1990. El Batolito de Colangüil, cordillera frontal de Argentina: estructura y marco tectónico. Revista Geológica de Chile 17 (1): 89-108. doi: 10.5027/andgeoV17n1-a04.

Llambías, E.J.; Sato, A.M. 1995. El Batolito de Colangüil: transición entre orogénesis y anorogénesis. Revista de la Asociación Geológica Argentina 50 (1-4): 111-131. Buenos Aires.

Llambías, E.J.; Kleiman, L.E.; Salvarredi, J.A. 1993. El Magmatismo Gondwánico. *In* Geología y Recursos Naturales de Mendoza (Ramos, V.; editor). Congreso Geológico Argentino, No. 12 y Congreso de Exploración de Hidrocarburos, No. 2. Relatorio: 53-64. Mendoza.

Llambías, E.J.; Quenardelle, S.; Montenegro, T. 2003. The Choiyoi Group from central Argentina: a subalkaline transitional to alkaline association in the craton adjacent to the active margin of the Gondwana continent. Journal of South American Earth Sciences 16: 243-257.

Ludwig, K.R. 2003. Isoplot/EX version 3.0, a geochronological toolkit for Microsoft Excel. Berkeley Geochronology Center, Special Publication.

Maksaev, V.; Munizaga, F.; Tassinari, C. 2014. Timing of the magmatism of the paleo-Pacific border of Gondwana: U-Pb geochronology of Late Paleozoic to Early Mesozoic igneous rocks of the north Chilean Andes between 20° and 31°S. Andean Geology 41 (3): 447-506. doi: 10.5027/andgeoV41n3-a01

Martin, M.W.; Clavero R., J.; Mpodozis, M., C. 1999. Late Paleozoic to Early Jurassic tectonic development of the high Andean Principal Cordillera, El Indio Region, Chile (29-30°S). Journal of South American Earth Sciences 12: 33-49.

Martínez, F.; Arriagada, C.; Mpodozis, C.; Peña, M. 2012. The Lautaro Basin: A record of inversion tectonics in northern Chile. Andean Geology 39 (2): 258-278. doi: http://dx.doi.org/10.5027/andgeoV39n2-a04.

Martínez, F.; Peña, M.; Arriagada, C. 2015. Geología del área Iglesia Colorada-Cerros del Potro y Cerro Mondaquita, región de Atacama. Servicio Nacional de Geología y Minería, Carta Geológica de Chile, Serie Geología Básica 179-180, 1 mapa escala 1:100.000. Santiago.

Morata, D.; Aguirre, L.; Oyarzún, M.; Vergara, M. 2000. Crustal contribution in the genesis of the bimodal Triassic volcanism from the Coastal Range, central Chile. Revista Geológica de Chile 27 (1): 83-98. doi: 10.5027/andgeoV27n1-a06.

Moscoso, R.; Mpodozis, C. 1988. Estilos estructurales en el norte chico de Chile (28-31°S), regiones de Atacama y Coquimbo. Revista Geológica de Chile 15 (2): 151-166. doi: 10.5027/andgeoV15n2-a04.

Moscoso, R.; Mpodozis, C.; Nasi, C.; Ribba, L.; Arévalo, C. 2010. Geología de la Hoja El Tránsito, Región de Atacama. Servicio Nacional de Geología y Minería, Carta Geológica de Chile, Serie Preliminar 7: 17 p., 1 mapa escala 1:250.000. Santiago.

Mpodozis, C.; Cornejo, P. 1988. Hoja Pisco Elqui, Región de Coquimbo. Servicio Nacional de Geología y Minería, Carta Geológica de Chile, Serie Geología Básica 68: 120 p., 1 mapa escala 1:250.000. Santiago.

Mpodozis, C.; Ramos, V. 1989. The Andes of Argentina and Chile. *In* Geology of the Andes and its relation to hydrocarbon and mineral resources (Ericksen, G.E.; Cañas Pinochet, M.T.; Reinemund, J.A.; editors). Circumpacific Council for Energy and Mineral Resources, Earth Science Series 11: 59-90.

Mpodozis, C.; Kay, S. 1992. Late Paleozoic to Triassic evolution of the pacific Gondwana margin: evidence from Chilean frontal Cordilleran batholiths. Geological Society of America Bulletin 104: 999-1014.

Nasi, C.; Mpodozis, C.; Moscoso, R.; Maksaev, V.; Cornejo, P. 1985. El Batolito Elqui-Limarí (Paleozoico Superior-Triásico): características petrográficas, geoquímicas y significado tectónico. Revista Geológica de Chile 25-26: 77-111. doi: 10.5027/andgeoV12n2-3-a06.

Nasi, C.; Moscoso, R.; Maksaev, V. 1990. Hoja Guanta. Servicio Nacional de Geología y Minería, Carta Geológica de Chile, Serie Geología Básica 67: 141 p., 1 mapa escala 1:250.000.

Ortiz, M.; Merino, R.N. 2015. Geología de las áreas Río Chollay-Matancilla y Cajón del Encierro, regiones de Atacama y Coquimbo. Servicio Nacional de Geología y Minería, Carta Geológica de Chile, Serie Geología Básica 175-176, 1 mapa escala 1:100.000.

Parada, F. 2013. Geoquímica de las rocas ígneas del Carbonífero-Triásico de la Alta Cordillera, Región de Atacama, Chile. Memoria de Título (Inédito), Universidad de Chile, Departamento de Geología: 93 p. Santiago.

Parada, M.A. 1981. Lower Triassic Alkaline Granites of Central Chile (30°S) in the High-Andean Cordillera. Geologische Rundschau 70: 1043-1053.

Parada, M.A. 1982. Petrology of the Lower Triassic anorogenic granites in the High Andes (30°S), Chile. Ph.D. Thesis (Unpublished). Tohoku University, 165 p. Japan.

Parada, M.A. 1984. La asociación de granitos subsolvus e hipersolvus del plutón Montegrande (Chile 30ºS) y el desarrollo de sus pertitas. Revista Geológica de Chile 23: 69-77. doi: http://dx.doi.org/10.5027/andgeoV11n3-a05.

Parada, M.A. 1988. Pre-Andean peraluminous and metaluminous leucogranitoid suites in the High Andes of Central Chile. Journal of South American Earth Sciences 1 (2): 211-221.

Parada, M.A.; Levi, B.; Nyström, J.O. 1991. Geochemistry of the Triassic to Jurassic plutonism of central Chile (30 to 33°S); Petrogenetic implications and a tectonic discussion. Geological Society of America, Special Paper 265: 99-112. doi: 10.1130/SPE265-p99.

Parada, M.A.; Levi, B.; Nyström, J.O. 1999. Multiple sources for the Coastal Batholith of central Chile (31-34°S): geochemical and Sr-Nd isotopic evidence and tectonic implications. Lithos 46: 505-521. doi: 10.1016/S0024-4937(98)00080-2.

Pearce, P.A.; Harris, N.B.W.; Tindle, A.G. 1984. Trace Element Discrimination Diagrams for the Tectonic Interpretation of Granitic Rocks. Journal of Petrology 25: 956-983. doi: 10.1093/petrology/25.4.956.

Peccerillo, A.; Taylor, S.R. 1976, Geochemistry of eocene calc-alkaline volcanic rocks from the Kastamonu area, northern Turkey. Contributions to Mineralogy and Petrology 58: 63-81.

Pichowiak, S.; Buchelt, M.; Damm, K.W. 1990. Magmatic activity and tectonic setting of early stages of Andean cycle in northern Chile. Geological Society of America, Special Paper 241: 127-144.

Pichowiak, S. 1994. Early Jurassic to Early Cretaceous magmatism in the Coastal Cordillera and the Central Depression of North Chile. *In* Tectonics of the Southern Central Andes (Reutter, K.J.; Scheuber, E.; Wigger, P.; Editors). Springer: 203-217. Heidelberg.

Pitcher, W.S. 1993. The Nature and Origin of Granite. Blackie: 321 p. London.

Pitcher, W.S.; Atherton, M.P.; Cobbing, E.J.; Beckensale (editors). 1985. Magmatism at a Plate Edge. The Peruvian Andes. Springer: 328 p. Berlin.

Poma, S.; Zappettini, E.O.; Quenardelle, S.; Santos, J.O.; Koukharsky, M.; Belousova, E.; McNaughton, N. 2014. Geochemistry, U-Pb SHRIMP zircon dating and Hf isotopes of the Gondwanan magmatism in NW Argentina: petrogenesis and geodynamic implications. Andean Geology 41: 267-292. doi: 10.5027/andgeoV41n2-a01.

Ramos, V.A.; Kay, S.M. 1991. Triassic rifting and associated basalts in the Cuyo basin, central Argentina. *In* Andean magmatism and its tectonic setting (Harmon, R.S.; Rapela, C.W.; editors). Geological Society of America, Special Papers 265: 79-91. Boulder.

Reutter, K.J. 1974. Entwicklung und Bauplan der chilenischen Hochkordillere im Bereich 29° südlicher Breite. Neues Jahrbuch für Geologie und Palaontologie 146: 153-178.

Ribba, L. 1985. Geología Regional del Cuadrángulo El Tránsito, Región de Atacama. Memoria de Título (Inédito), Universidad de Chile: 203 p. Santiago.

Ribba, L.; Mpodozis, C.; Hervé, F.; Nasi, C.; Moscoso, R. 1988. El basamento del valle del Tránsito, Cordillera de Vallenar: eventos magmáticos y metamórficos y su relación con la evolución paleozoica de los Andes Chileno-Argentinos. Revista Geológica de Chile 15 (2): 129-149. doi: 10.5027/andgeoV15n2-a03.

Rogers, G.; Hawkesworth, C.J. 1989. A geochemical traverse across the North Chilean Andes: Evidence for crust generation melt from the mantle wedge. Earth and Planetary Science Letters 91: 271-285.

Rossel, P.; Oliveros, V.; Ducea, M.; Charrier, R.; Scaillef, S.; Retamal, L.; Figueroa, O. 2013. The Early Andean Subduction system as an analogue to island arcs: evidence from across-arc geochemical variations in northern Chile. Lithos 179: 211-230. doi: 10.1016/j.lithos.2013.08.014.

Salazar, E.; Coloma, F.; Creixell, C. 2013. Geología del área El Tránsito-Lagunillas, Región de Atacama. Servicio Nacional de Geología y Minería, Carta Geológica de Chile, Serie Geología Básica 149: 121 p., 1 mapa 1:100.000.

Salazar, E.; Coloma, F. 2016. Geología del área Cerros de Cantaritos-Laguna Chica, Región de Atacama. Servicio Nacional de Geología y Minería, Carta Geológica de Chile, Serie Geología Básica 181: 171 p., 1 mapa 1:100.000.

Sepúlveda, F.; Vásquez, P.; Quezada, A. 2014. Cartas Patillos y Oficina Victoria, Región de Tarapacá. Servicio Nacional de Geología y Minería, Carta Geológica de Chile, Serie Geología Básica 167-168: 1 mapa 1:100.000.

Shand, S.J. 1927. The eruptive rocks. John Wiley: 488 p. New York.

Spalletti, L.A. 1997. Western Argentinian Triassic basin: origin and evolution. Acta Geologica Hispanica 32: 29-50.

Spalletti, L.A.; Fanning, C.M.; Rapela, C.W. 2006. Dating the Triassic continental rift in the southern Andes: the Potrerillos Formation, Cuyo Basin, Argentina. Geologica Acta 6: 267-283. doi: 10.1344/105.000000256.

Stacey, J.S.; Kramers, J.D. 1975. Approximation of terrestrial lead isotope evolution by a two-stage model. Earth and Planetary Science Letters 26: 207-221.

Stern, R.J. 2002. Subduction zones. Reviews in Geophysics 40: 1012. doi: 10.1029/2001RG000108.

Sun, S.S.; McDonough, W.F. 1989. Chemical and isotopic systematics of oceanic basalts: implications for mantle composition and processes. Geological Society, Special Publication 42: 313-345.

Valin, X. 2014. Geoquímica de las unidades del Triásico a Jurásico Inferior en el norte de Chile (28º00´-29º30´S): implicancias para el inicio de la subducción. Memoria

de Título (Inédito), Universidad de Concepción, Departamento de Ciencias de la Tierra: 104 p. Concepción.

Vallejos, D. 2014. Estudio sedimentológico y estructural de la Formaciones Canto de Agua, San Félix, La Totora y Estratos del Verraco: implicancia en la evolución triásica del margen andino. Memoria de Título (Inédito), Universidad de Concepción, Departamento de Ciencias de la Tierra: 104 p. Concepción.

Vásquez, P.; Glodny, J.; Franz, G.; Frei, D.; Romer, R.L. 2011. Early Mesozoic plutonism of the Cordillera de la Costa (34º-37ºS), Chile: Constraints on the onset of the Andean Orogeny. The Journal of Geology 119 (2): 159-184.

Welkner, D.; Arévalo, C.; Godoy, E. 2006. Geología del área Freirina-El Morado, Región de Atacama. Servicio Nacional de Geología y Minería, Carta Geológica de Chile, Serie Geología Básica 100: 50 p., 1 mapa 1:100.000.

Winchester, J.A.; Floyd, P.A. 1977. Geochemical discrimination of different magma series and their differentiation products using immobile elements. Chemical Geology 20: 325-343.

Winter, J.D. 2010. An introduction to igneous and metamorphic petrology, 2nd ed. Pearson Prentice Hall: 702 p. New Jersey.

Manuscript received: May 20, 2016; revised/accepted: November 21, 2016; available online: November 21, 2016.

APPENDIX 1. SUMMARY OF THE PETROGHRAPHIC DESCRIPTION OF THE STUDIED SAMPLES.

Sample	Lithology	UTM		Unit	Igneous components																					Alteration minerals									
		E	N		Phn	Gls	Lith	Gdms	Mtr	TOTAL	Pl	Qz	Ort	Mic	Bt	Amp	Mv	Cpx	Opx	Ol	Indet	Opa	Sph	Ap	Rut	TOTAL	Q	A	P	Cc	Ser	Chl	Ep	Qz	Prh	Cl	Bt	Fe-mx	TOTAL
CPV-12-105	Rhyolite	286,402	6,789,103	Llano de Chocolate Beds	0.05	0	0	0.95	0	1	0	0.15	0	0	0	0	0	0	0	0	0.05	0	0	0	0	0.20	0.00	0.00	0.00	0.12	0	0	0	0.65	0	0	0.03	0	0.80
CPV-12-12	Dacite	289,084	6,794,562	Llano de Chocolate Beds	0.4	0.2	0	0.4	0	1	0.05	0.4	0.3	0	0	0	0	0	0	0	0	0	0	0	0	0.75	0.00	0.00	0.00	0	0.1	0.1	0.02	0.02	0	0	0	0.01	0.25
CPV-12-127	Tuff rhyolitic	287,052	6,792,338	Llano de Chocolate Beds	0.4	0	0	0.6	0	1	0.11	0.39	0.21	0	0.05	0	0	0	0	0	0	0	0	0	0	0.76	0.00	0.00	0.00	0.1	0.02	0.01	0	0.08	0	0	0.01	0.02	0.24
ST-04t	Tonalite	374,082	6,825,547	Chanchoquín Plutonic Complex	1	0	0	0	0	1	0.4	0.5	0.005	0	0.03	0	0.01	0	0	0	0	0.02	0	0	0	0.96	0.55	0.00	0.44	0	0.02	0.01	0.01	0	0	0	0	0	0.04
CT-310t	Granodiorite	368,483	6,801,578	Chanchoquín Plutonic Complex	1	0	0	0	0	1	0.33	0.37	0.16	0	0.01	0	0.02	0	0	0	0	0.005	0.005	0	0	0.90	0.43	0.19	0.38	0	0.04	0.03	0.02	0	0	0.01	0	0	0.10
CT-311t	Granodiorite	367,097	6,802,740	Chanchoquín Plutonic Complex	1	0	0	0	0	1	0.39	0.31	0.15	0	0.025	0.035	0	0	0	0	0	0.015	0.005	0	0	0.93	0.36	0.18	0.46	0	0.05	0.02	0	0	0	0	0	0	0.07
CT-340t	Tonalite	374,514	6,825,661	Chanchoquín Plutonic Complex	1	0	0	0	0	1	0.37	0.38	0.05	0.05	0.01	0	0	0	0	0	0	0.01	0	0	0	0.87	0.45	0.12	0.44		0.03	0.06	0.03	0	0	0.01	0	0	0.13
CT-91t	Tonalite	379,800	6,830,776	Chanchoquín Plutonic Complex	1	0	0	0	0	1	0.37	0.37	0.1	0	0	0	0.08	0	0	0	0	0.01	0	0	0	0.93	0.44	0.12	0.44	0	0.06	0.01	0	0	0	0	0	0	0.07
ST-70t	Tonalite	374,529	6,815,397	Chanchoquín Plutonic Complex	1	0	0	0	0	1	0.39	0.5	0.005	0	0.025	0	0.01	0.01	0	0	0	0.015	0	0.005	0	0.96	0.56	0.01	0.44	0	0.02	0	0.02	0	0	0.005	0	0	0.04
ST-71t	Tonalite	374,343	6,823,076	Chanchoquín Plutonic Complex	1	0	0	0	0	1	0.62	0.2	0.02	0	0.03	0.08	0	0	0	0	0	0.02	0	0	0	0.97	0.24	0.02	0.74	0	0.01	0.01	0	0	0.01	0	0	0	0.03
CT-236t	Tonalite	369,825	6,794,058	Chanchoquín Plutonic Complex	1	0	0	0	0	1	0.41	0.36	0.09	0	0	0	0.02	0	0	0	0	0.04	0	0	0	0.92	0.42	0.10	0.48	0	0.07	0	0	0	0.01	0	0	0	0.08
CT-334t	Tonalite	373,490	6,822,573	Chanchoquín Plutonic Complex	1	0	0	0	0	1	0.4	0.35	0.05	0	0	0	0.04	0	0	0	0	0.015	0	0	0	0.86	0.44	0.06	0.50	0	0.13	0	0	0	0	0.015	0	0	0.15
CT-337t	Tonalite	373,821	6,822,372	Chanchoquín Plutonic Complex	1	0	0	0	0	1	0.68	0.02	0.02	0	0	0.1	0	0	0	0	0	0.02	0	0	0	0.84	0.03	0.03	0.94	0	0.05	0.1	0.01	0	0	0	0	0	0.16
07-15	Tonalite	366,163	6697,056	Guanta Unit	1	0	0	0	0	1	0.34	0.38	0	0.01	0.11	0.16	0	0	0	0	0	0	0	0	0	1.00	0.52	0.01	0.47	0	0	0	0	0	0	0	0	0	0.00
ST-69t	Dike	374,199	6,825,644	Dike-Chanchoquín Plutonic Complex	0.1	0	0	0.9	0	1	0.45	0.45	0.005	0	0	0	0	0	0	0	0	0	0	0	0	0.90	0.00	0.00	0.00	0.01	0.09	0	0	0	0	0	0	0	0.10
CT-160t	Tonalite	395,024	6,818,536	Quebrada El Pintado Tonalites	1	0	0	0	0	1	0.37	0.51	0.005	0	0.035	0	0.02	0	0	0	0	0.01	0	0.005	0	0.95	0.58	0.01	0.42	0	0.03	0.01	0.01	0	0	0	0	0	0.05
CT-202t	Tonalite	403,497	6,825,929	Quebrada El Pintado Tonalites	1	0	0	0	0	1	0.56	0.22	0.005	0	0.04	0.09	0	0	0	0	0	0.02	0.01	0	0	0.94	0.28	0.01	0.71	0	0.03	0.01	0.01	0	0.01	0	0	0	0.06
CT-296t	Tonalite	385,541	6,815,785	Quebrada El Pintado Tonalites	1	0	0	0	0	1	0.59	0.24	0.04	0	0.03	0	0	0.01	0	0	0	0.01	0	0	0	0.92	0.28	0.05	0.6,8	0	0.05	0.01	0.01	0	0	0.01	0	0	0.08
ST-97t	Tonalite	402,086	6,818,320	Quebrada El Pintado Tonalites	1	0	0	0	0	1	0.45	0.49	0.005	0	0.03	0	0	0	0	0	0	0.01	0	0	0	0.98	0.52	0.00	0.48	0	0.01	0.01	0	0	0	0	0	0	0.02
CT-213t	Dacite	398,529	6,829,454	Guanaco Sonso Fm	0.15	0	0.85	0	0	1	0.55	0.08	0	0	0	0	0	0	0	0	0	0.02	0	0	0	0.65	0.00	0.00	0.00	0.05	0	0.08	0.05	0.15	0	0	0.02	0	0.35
CT-216t	Basalt	398,566	6,826,902	Guanaco Sonso Fm	0.15	0	0.85	0	0	1	0.6	0	0	0	0	0.04	0	0.01	0	0	0	0.1	0	0	0	0.75	0.00	0.00	0.00	0.05	0	0.1	0	0	0	0	0.1	0	0.25
ST-13t	Basalt	391,425	6,832,423	Guanaco Sonso Fm		0	0	1	0	1	0.7	0	0	0	0	0	0	0	0	0	0	0.05	0	0	0	0.75	0.00	0.00	0.00	0.05	0	0.1	0	0	0	0	0.1	0	0.25
ST-14t	Rhyolite	391,157	6,832,231	Guanaco Sonso Fm	0.4	0.1	0.5	0	0	1	0	0.55	0.15	0	0	0	0	0	0	0	0	0.05	0	0	0	0.75	0.00	0.00	0.00	0.05	0.05	0.05	0	0	0	0	0.1	0	0.25
CT-286t	Basaltic andesite	392,912	6,831,276	Guanaco Sonso Fm	0.15	0	0	0.85	0	1	0.72	0	0	0	0	0.12	0	0	0	0	0	0.03	0	0	0	0.87	0.00	0.00	0.00	0	0.06	0.02	0	0	0	0	0.05	0	0.13
07-10	Gabbro	396,451	6669,570	La Laguna Gabbro	1	0	0	0	0	1	0.65	0.01	0.05	0	0	0	0	0.2	0	0	0	0.09	0	0	0	1.00	0.01	0.07	0.92	0	0	0	0	0	0	0	0	0	0.00
07-11	Gabbro	396,266	6669,913	La Laguna Gabbro	1	0	0	0	0	1	0.53	0.02	0.05	0	0	0	0	0.25	0.05	0	0	0.05	0	0	0	0.95	0.03	0.08	0.88	0	0.02	0.03	0	0	0	0	0	0	0.05
CT-228t	Granodiorite	399,350	6,827,873	Chollay Plutonic Complex	1	0	0	0	0	1	0.335	0.37	0.165	0	0.035	0.02	0	0	0	0	0	0.01	0	0	0	0.94	0.43	0.19	0.39	0	0.05	0.01	0	0	0	0.005	0	0	0.07
ST-16t	Granodiorite	381,935	6,793,400	Chollay Plutonic Complex	1	0	0	0	0	1	0.36	0.53	0.02	0	0.015	0	0.02	0	0	0	0	0.005	0	0	0	0.95	0.58	0.02	0.40	0	0.04	0.01	0	0	0	0	0	0	0.05
CT-19t	Granodiorite	383,379	6,824,951	Chollay Plutonic Complex	1	0	0	0	0	1	0.35	0.5	0.05	0	0.03	0	0	0	0	0	0	0.01	0	0	0	0.94	0.56	0.06	0.39	0	0.04	0.01	0.005	0	0	0.005	0	0	0.06
CT-237t	Granodiorite	390,947	6,805,063	Chollay Plutonic Complex	1	0	0	0	0	1	0.44	0.41	0.05	0	0.01	0	0	0	0	0	0	0.015	0	0.005	0	0.93	0.46	0.06	0.49	0	0.04	0.015	0.01	0	0	0.005	0	0	0.07
CT-284t	Granodiorite	398,488	6,832,391	Chollay Plutonic Complex	1	0	0	0	0	1	0.4	0.34	0.07	0	0	0	0	0	0	0	0	0.02	0	0	0	0.83	0.42	0.09	0.49	0	0.15	0	0	0	0	0.02	0	0	0.17
ST-160t	Granodiorite	380,014	6,826,448	Chollay Plutonic Complex	1	0	0	0	0	1	0.55	0.27	0.03	0	0.02	0.02	0	0	0	0	0	0.02	0	0	0	0.91	0.32	0.04	0.65	0	0.06	0.03	0	0	0	0	0	0	0.09
CT-191t	Granodiorite	386,550	6,800,942	Chollay Plutonic Complex	1	0	0	0	0	1	0.415	0.38	0.04	0	0.06	0.025	0	0	0	0	0	0.01	0	0	0.005	0.94	0.46	0.05	0.50	0	0.045	0.005	0.01	0	0.005	0	0	0	0.07
CT-19Bt	Granodiorite	383,379	6,824,951	Chollay Plutonic Complex	1	0	0	0	0	1	0.47	0.38	0.04	0	0.035	0	0	0	0	0	0	0.015	0	0	0	0.94	0.43	0.04	0.53	0	0.05	0.01	0	0	0	0	0	0	0.06
CT-154t	Granodiorite	402,037	6,814,985	Chollay Plutonic Complex	1	0	0	0	0	1	0.49	0.37	0.07	0	0.035	0	0	0	0	0	0	0.01	0.005	0.002	0.003	0.99	0.40	0.08	0.53	0	0.005	0	0.01	0	0	0	0	0	0.02
SCL-02t	Monzogranite	410,948	6,804,964	Chollay Plutonic Complex	1	0	0	0	0	1	0.25	0.33	0.32	0	0.02	0	0.01	0	0	0	0	0.01	0	0	0	0.94	0.37	0.36	0.28	0	0.03	0.005	0	0	0	0.01	0.01	0	0.005	0.06
CT-146At	Monzogranite	401,863	6,792,472	Chollay Plutonic Complex	1	0	0	0	0	1	0.245	0.37	0.28	0	0.01	0	0.005	0	0	0	0	0.015	0	0	0	0.93	0.41	0.31	0.27	0	0.04	0.015	0.005	0	0	0.015	0	0	0.08
CT-158t	Monzogranite	397,408	6,818,476	Chollay Plutonic Complex	1	0	0	0	0	1	0.27	0.3	0.26	0.05	0.01	0	0.01	0	0	0	0	0.015	0	0	0	0.92	0.34	0.35	0.31	0	0.045	0.02	0.005	0	0	0.015	0	0	0.09
CT-161t	Monzogranite	393,442	6,815,293	Chollay Plutonic Complex	1	0	0	0	0	1	0.29	0.33	0.26	0	0.015	0	0.015	0	0	0	0	0.015	0	0	0	0.93	0.38	0.30	0.33	0	0.035	0.015	0.01	0	0	0.015	0	0	0.08
CT-196t	Monzogranite	387,555	6,792,323	Chollay Plutonic Complex	1	0	0	0	0	1	0.2	0.38	0.21	0.09	0.02	0	0.005	0	0	0	0	0.015	0	0	0	0.92	0.43	0.34	0.23	0	0.05	0.01	0.005	0	0	0.015	0	0	0.08
CT-199t	Monzogranite	408,498	6,829,131	Chollay Plutonic Complex	1	0	0	0	0	1	0.25	0.3	0.3	0.07	0.02	0	0	0	0	0	0	0.01	0	0	0	0.95	0.33	0.40	0.27	0	0.03	0.01	0	0	0	0.01	0	0	0.05
CT-233t	Monzogranite	403,253	6,827,221	Chollay Plutonic Complex	1	0	0	0	0	1	0.25	0.335	0.305	0	0	0	0.02	0	0	0	0	0.015	0	0	0	0.93	0.38	0.34	0.28	0	0.06	0.005	0	0	0	0.01	0	0	0.08
CT-290t	Monzogranite	392,242	6,829,713	Chollay Plutonic Complex	1	0	0	0	0	1	0.315	0.29	0.285	0.03	0.005	0	0	0	0	0	0	0.01	0	0	0	0.94	0.32	0.34	0.34	0	0.04	0.025	0	0	0	0	0	0	0.07

Appendix 1 continued.

Sample	Lithology	Location		Unit	Igneous components																					Alteration minerals										
		E	N		Phn	Gls	Lith	Gdms	Mtr	TOTAL	Pl	Qz	Ort	Mic	Bt	Amp	Mv	Cpx	Opx	Ol	Indet	Opa	Sph	Ap	Rut	TOTAL	Q	A	P	Cc	Ser	Chl	Ep	Qz	Prh	Cl	Bt	Fe-mx	TOTAL
CT-233t	Monzogranite	403,253	6,827,221	Chollay Plutonic Complex	1	0	0	0	0	1	0.25	0.335	0.305	0	0	0	0.02	0	0	0	0	0.015	0	0	0	0.93	0.38	0.34	0.28	0	0.06	0.005	0	0	0	0.01	0	0	0.08
CT-290t	Monzogranite	392,242	6,829,713	Chollay Plutonic Complex	1	0	0	0	0	1	0.315	0.29	0.285	0.03	0.005	0	0	0	0	0	0	0.01	0	0	0	0.94	0.32	0.34	0.34	0	0.04	0.025	0	0	0	0	0	0	0.07
CT-291t	Monzogranite	392,172	6,829,943	Chollay Plutonic Complex	1	0	0	0	0	1	0.25	0.325	0.27	0.02	0	0	0	0	0	0	0	0.03	0	0	0	0.90	0.38	0.34	0.29	0.01	0.045	0.03	0.01	0	0	0.02	0	0	0.12
CT-294t	Monzogranite	385,861	6,815,848	Chollay Plutonic Complex	1	0	0	0	0	1	0.515	0.29	0.09	0.02	0.005	0	0	0	0	0	0	0.015	0	0	0	0.94	0.32	0.12	0.56	0	0.025	0.02	0	0	0	0.02	0	0	0.07
ST-80t	Monzogranite	386,379	6,794,246	Chollay Plutonic Complex	1	0	0	0	0	1	0.18	0.39	0.36	0.02	0.005	0	0.005	0	0	0	0	0.005	0	0	0	0.97	0.41	0.40	0.19	0	0.02	0.005	0	0	0	0.01	0	0	0.04
ST-98Bt	Monzogranite	399,244	6,819,375	Chollay Plutonic Complex	1	0	0	0	0	1	0.22	0.53	0.16	0.02	0.03	0	0	0	0	0	0	0.01	0.005	0	0	0.98	0.57	0.19	0.24	0	0.02	0	0.005	0	0	0	0	0	0.03
ST-17t	Monzogranite	399,663	6,795,057	Chollay Plutonic Complex	1	0	0	0	0	1	0.22	0.34	0.3	0.04	0	0	0.005	0	0	0	0	0.015	0	0	0	0.92	0.38	0.38	0.24	0	0.045	0.015	0.005	0	0	0.015	0	0	0.08
SCL-09t	Tonalite	410,315	6,794,865	Chollay Plutonic Complex	1	0	0	0	0	1	0.4	0.3	0.1	0	0.035	0.07	0	0	0	0	0	0.015	0.015	0	0	0.94	0.38	0.13	0.50	0	0.045	0.01	0	0	0	0.01	0	0	0.07
CT-164t	Tonalite	389,794	6,810,101	Chollay Plutonic Complex	1	0	0	0	0	1	0.53	0.21	0.005	0	0	0.08	0	0	0	0	0	0.035	0.005	0	0	0.86	0.28	0.01	0.71	0	0.1	0.03	0.01	0	0	0	0	0	0.14
CT-167t	Tonalite	384,487	6,804,556	Chollay Plutonic Complex	1	0	0	0	0	1	0.52	0.15	0.005	0	0.04	0.17	0	0	0	0	0	0.02	0	0.005	0	0.91	0.22	0.01	0.77	0	0.04	0.02	0.01	0	0.02	0	0	0	0.09
CT-173t	Tonalite	381,395	6,792,135	Chollay Plutonic Complex	1	0	0	0	0	1	0.37	0.2	0.005	0	0	0.11	0	0	0	0	0	0.03	0.01	0.01	0	0.73	0.35	0.01	0.64	0	0.13	0.1	0.02	0	0.02	0	0	0	0.27
CT-250t	Tonalite	384,825	6,797,022	Chollay Plutonic Complex	1	0	0	0	0	1	0.48	0.36	0.01	0	0.04	0	0.03	0	0	0	0	0.01	0	0	0	0.93	0.42	0.01	0.56	0	0.06	0.01	0	0	0	0	0	0	0.07
CT-255t	Tonalite	382,332	6,799,818	Chollay Plutonic Complex	1	0	0	0	0	1	0.485	0.36	0.02	0	0.045	0	0.04	0	0	0	0	0.01	0	0	0	0.96	0.42	0.02	0.56	0	0.035	0.005	0	0	0	0	0	0	0.04
CT-300t	Tonalite	395,358	6,793,507	Chollay Plutonic Complex	1	0	0	0	0	1	0.57	0.22	0.005	0	0.05	0.05	0	0.02	0	0	0	0.02	0	0	0	0.93	0.28	0.01	0.72	0	0.06	0	0	0	0	0.01	0	0	0.07
CT-35t	Tonalite	382,678	6,791,765	Chollay Plutonic Complex	1	0	0	0	0	1	0.58	0.28	0.005	0	0.075	0	0	0	0	0	0	0.01	0	0.005	0	0.95	0.32	0.01	0.67	0	0.04	0.005	0.005	0	0	0	0	0	0.05
CT-193t	Gabbro-Diorite	387,560	6,800,338	Chollay Plutonic Complex	1	0	0	0	0	1	0.54	0.03	0.02	0	0.07	0.22	0	0	0	0	0	0.01	0	0	0	0.89	0.05	0.03	0.92	0	0.1	0	0.005	0	0.005	0	0	0	0.11
CPV-12-38*	Tuff lithic	362,530	6,778,657	San Félix Formation	0	0.1	0.6	0	0.3	1	0.1	0.2	0	0	0	0	0	0	0	0	0	0	0	0	0	0.30	0.00	0.00	0.00	0	0.1	0	0.06	0.4	0	0.1	0.02	0.02	0.70
CPV-12-49b*	Tuff lithic	359,174	6,805,415	San Félix Formation	0.3	0.3	0	0	0.4	1	0.15	0.3	0.05	0	0	0	0	0	0	0	0	0	0	0	0	0.50	0.00	0.00	0.00	0	0.15	0.1	0	0.2	0	0	0	0.05	0.50
CT-75At	Tuff andesitic	359,175	6,802,616	San Félix Formation	0.15	0.05	0.15	0	0.65	1	0.22	0.28	0	0	0	0	0.02	0	0	0	0	0.02	0	0	0	0.54	0.00	0.00	0.00	0.02	0.1	0.1	-	0.2	0	0.03	0	0.01	0.46
ST-212At	Tuff	359,089	6,803,160	San Félix Formation	0.1	0.05	0.1	0	0.8	1	0.03	0.35	0.01	0	0	0	0	0	0	0	0	0.005	0	0	0	0.40	0.00	0.00	0.00	0.15	0.2	0.05	0	0.2	0	0	0	0	0.60
SCL-14t	Sienogranite	417,451	6,798,699	Colorado Syenogranite	1	0	0	0	0	1	0.24	0.35	0.26	0.025	0.02	0	0	0	0	0	0	0.015	0	0	0	0.91	0.40	0.33	0.27	0	0.04	0.01	0.01	0	0	0.03	0	0	0.09
ST-94t	Sienogranite	399,882	6,809,628	Colorado Syenogranite	1	0	0	0	0	1	0.16	0.43	0.33	0.01	0	0	0.01	0	0	0	0	0.01	0	0	0	0.95	0.46	0.37	0.17	0	0.03	0.01	0	0	0	0.01	0	0	0.05
CT-74t	Dike	359,296	6,802,576	Dike-San Félix Formation	0.1	0	0	0.9	0	1	0.58	0.02	0.005	0	0	0	0	0	0	0	0	0	0	0	0	0.60	0.00	0.00	0.00	0.05	0.08	0.2	0.02	0	0	0.05	0	0	0.40
ST-93At	Tuff andesitic	386,440	6,829,587	La Totora Formation	0.19	0.08	0.2	0	0.53	1	0.05	0.02	0.03	0	0	0.02	0	0	0	0	0.08	0.03	0	0	0	0.23	0.00	0.00	0.00	0	0.3	0	0	0.35	0.02	0.1	0	0	0.77
ST-196t	Tuff rhyolithic	388,721	6,839,736	La Totora Formation	0.1	0.07	0.3	0	0.53	1	0.06	0.01	0	0	0	0	0	0	0	0	0.05	0.02	0	0	0	0.14	0.00	0.00	0.00	0.03	0.2	0.08	0.05	0.45	0	0.05	0	0	0.86
ST-11t	Andesite	378,863	6,818,138	La Totora Formation	0.2	0	0	0.8	0	1	0.75	0	0	0	0	0	0	0	0.03	0	0	0	0.03	0	0	0.81	0.00	0.00	0.00	0.1	0	0.02	0	0	0	0.05	0	0.02	0.19
ST-190t	Andesite	392,312	6,838,728	La Totora Formation	0.05	0	0	0.95	0	1	0.82	0	0	0	0	0	0	0	0	0	0	0	0.1	0	0	0.92	0.00	0.00	0.00	0.07	0	0	0	0	0	0.01	0	0	0.08
CPV-12-23	Andesite	376,484	6,814,323	La Totora Formation	0.05	0	0	0.95	0	1	0.7	0	0	0	0	0	0	0.1	0	0	0	0.05	0	0	0	0.85	0.00	0.00	0.00	0	0	0	0	0	0	0	0	0.15	0.15
CPV-12-24	Andesite	383,333	6,826,718	La Totora Formation	0.05	0	0	0.95	0	1	0.52	0	0	0	0	0.03	0	0	0	0.03	0.1	0	0	0	0	0.68	0.00	0.00	0.00	0.07	0	0.1	0	0	0	0	0	0.15	0.32
CPV-12-60	Basalt	382,348	6,827,655	La Totora Formation	0.68	0.32	0	0	0	1	0.76	0	0	0	0	0	0	0	0	0	0	0.06	0	0	0	0.82	0.00	0.00	0.00	0.08	0	0	0	0	0	0.1	0	0	0.18
SCL-26q*	Tuff	414,172	6,808,064	La Totora Formation	0.05	0.03	0.02	0	0.9	1	0.02	0.03	0	0	0	0	0	0	0	0	0.05	0.01	0	0	0	0.11	0.00	0.00	0.00	0.2	0.1	0.02	0	0.5	0	0.07	0	0	0.89
ST-62t	Rhyolite	363,165	6,823,706	La Totora/San Félix Formation	0.4	0.02	0.05	0	0.53	1	0.15	0.15	0	0	0	0	0	0	0	0	0.02	0.02	0	0	0	0.34	0.00	0.00	0.00	0.07	0.1	0.01	0	0.45	0	0.03	0	0	0.66
ST-175t	Tuff rhyolithic	362,224	6,814,186	La Totora/San Félix Formation	0.15	0.1	0.4	0	0.35	1	0.55	0.08	0	0	0	0	0	0	0	0	0.1	0.03	0	0	0	0.76	0.00	0.00	0.00	0.02	0.05	0.05	0	0.05	0	0.02	0	0.05	0.24
ST-43t	Basalt	362,923	6,811,342	La Totora/San Félix Formation	0	0.1	0	0.9	0	1	0.63	0	0	0	0	0	0	0	0	0.02	0.05	0.05	0	0	0	0.75	0.00	0.00	0.00	0.1	0.05	0.1	0	0	0	0	0	0	0.25
07-07	Granite	361,047	6,666,761	Monte Grande Unit	1	0	0	0	0	1	0.15	0.3	0.4	0	0.04	0.07	0	0.04	0	0	0	0	0	0	0	1.00	0.35	0.47	0.18	0	0	0	0	0	0	0	0	0	0.00
07-06	Granite	357,424	6,668,630	Monte Grande Unit	1	0	0	0	0	1	0.25	0.3	0.1	0.2	0.03	0.05	0	0	0	0	0.05	0	0	0	0	0.98	0.35	0.35	0.29	0	0.01	0.01	0	0	0	0	0	0	0.02
07-13	Granite (two-mica)	368,473	6,695,942	Los Tilos Granite	1	0	0	0	0	1	0.27	0.36	0.14	0	0.1	0.07	0.06	0	0	0	0	0	0	0	0	1.00	0.47	0.18	0.35	0	0	0	0	0	0	0	0	0	0.00
CPV-12-91A	Diorite	301,526	6,884,546	Carrizal Bajo Plutonic Complex	1	0	0	0	0	1	0.39	0.15	0.003	0	0	0.2	0	0	0	0	0	0.03	0	0	0	0.77	0.28	0.01	0.72	0	0.02	0.1	0.01	0	0	0.1	0	0	0.23
CPV-12-91B	Tonalite	301,526	6,884,546	Carrizal Bajo Plutonic Complex	1	0	0	0	0	1	0.34	0.38	0.004	0	0.08	0	0	0	0	0	0	0.02	0.02	0	0	0.84	0.52	0.01	0.47	0	0.02	0.03	0.01	0	0	0.1	0	0	0.16
CPV-12-93	Granodiorite	288,859	6,878,634	Carrizal Bajo Plutonic Complex	1	0	0	0	0	1	0.43	0.28	0.14	0	0.1	0	0	0	0	0	0	0	0	0	0	0.95	0.33	0.16	0.51	0	0	0	0	0	0	0.05	0	0	0.05
CPV-12-92	Diorite	298,038	6,887,501	Algodones Granite	1	0	0	0	0	1	0.34	0.09	0.005	0	0.03	0	0	0.12	0	0	0	0.02	0	0	0	0.60	0.21	0.01	0.78	0	0.1	0.1	0.05	0	0	0.15	0	0	0.40

Table listing the mineral components of the studied rocks expressed as % of volume of the total rock. The first and third TOTAL columns refer to the total amount of igneous and alteration components, respectively, present in the rock, regardless of the domain in which they occur. The second TOTAL column refers to the different igneous minerals detectable at micro scale. In the case of phaneritic rocks, igneous crystals are listed in the column "phenocrysts". **Phn**: Phenocyrsts; **Gls**: Glass; **Lith**: Lithics; **Gdms**: Groundmass; **Mtr**: Matrix; **Pl**: plagioclase; **Qz**: quartz; **Ort**: orthoclase; **Mic**: microcline; **Bt**: biotite; **Amp**: amphibole; **Mv**: muscovite; **Cpx**: clinopyroxene; **Opx**: orthopyroxene; **Ol**: olivine, **Indet**; mafic undetermined; **opa**: opaque mineral undetermined; **Sph**: sphene; **Ap**: apatite; **Rut**: rutile; **Q**: quartz; **A**: alkaline feldspar; **P**: plagioclase (for Streickesen classification of phaneritic rocks with % of mafic minerals under 90%); **Cc**: calcite/carbonate undetermined; **Ser**: sericite; **Chl**: chlorite; **Ep**: epidote; **Qz**: quartz (chalcedony, amorphous silica); **Prh**: prehnite; **Cl**: clay minerals; **Bt**: biotite; **Fe-ox**: Fe oxides/hydroxides.

* very alterated samples, which have not separated lithic fragments.

APPENDIX 2. U-Pb GEOCHRONOLOGIC ANALYSES.

Sample: 07-07	UTM N	6,666,761	UTM E	361,047	Unit	Monte Grande Unit	Isotope ratios								Apparent ages (Ma)				
Analysis	U (ppm)	$^{206}Pb/^{204}Pb$	U/Th	$^{206}Pb^*/^{207}Pb^*$	± (1σ) (%)	$^{207}Pb^*/^{235}U^*$	± (1σ) (%)	$^{206}Pb^*/^{238}U$	± (1σ) (%)	error corr.	$^{206}Pb^*/^{238}U^*$	± (1σ) (Ma)	$^{207}Pb^*/^{235}U$	± (1σ) (Ma)	$^{206}Pb^*/^{207}Pb^*$	± (1σ) (Ma)	Best age (Ma)	± (1σ) (Ma)	Conc (%)
07-07-19 <>	527.541	79,028.068	0.862	19.726	1.340	0.231	2.353	0.033	1.935	0.822	209.745	3.992	211.158	4.486	226.938	30.962	209.745	3.992	NA
07-07-11C <>	122.516	23,216.810	1.014	19.174	7.222	0.238	7.706	0.033	2.689	0.349	209.912	5.554	216.787	15.044	292.105	165.112	209.912	5.554	NA
07-07-12C <>	836.523	11,587.966	0.808	19.628	1.984	0.233	2.160	0.033	0.855	0.396	210.685	1.772	212.984	4.151	238.495	45.734	210.685	1.772	NA
07-07-18C <>	111.893	18,730.740	0.854	21.176	12.614	0.217	12.931	0.033	2.845	0.220	210.978	5.905	199.094	23.382	60.535	301.597	210.978	5.905	NA
07-07-1C <>	125.970	23,574.684	0.100	19.550	10.365	0.235	10.603	0.033	2.234	0.211	211.276	4.644	214.300	20.487	247.645	239.194	211.276	4.644	NA
07-07-17C <>	40.046	9,669.117	0.878	20.376	37.154	0.227	37.407	0.034	4.343	0.116	212.465	9.077	207.506	70.316	151.557	898.347	212.465	9.077	NA
07-07-2C <>	710.428	70,056.259	1.135	19.835	1.429	0.233	1.930	0.034	1.297	0.672	212.900	2.717	213.004	3.708	214.180	33.106	212.900	2.717	NA
07-07-10C <>	190.002	11,487.495	0.808	19.814	5.336	0.234	5.885	0.034	2.481	0.422	213.191	5.203	213.484	11.331	216.721	123.616	213.191	5.203	NA
07-07-15C <>	295.799	17,254.335	0.761	19.049	4.363	0.244	4.768	0.034	1.924	0.403	213.762	4.044	221.728	9.498	307.130	99.405	213.762	4.044	NA
07-07-3C <>	98.972	57,479.337	0.946	21.766	15.385	0.214	15.781	0.034	3.514	0.223	213.865	7.392	196.635	28.219	-5.383	373.063	213.865	7.392	NA
07-07-13C <>	793.885	40,790.281	0.633	19.092	3.757	0.244	4.260	0.034	2.007	0.471	214.044	4.225	221.537	8.478	301.875	85.677	214.044	4.225	NA
07-07-4C <>	80.608	14,980.416	1.121	19.730	13.507	0.236	13.928	0.034	3.396	0.244	214.046	7.151	215.084	27.002	226.479	313.397	214.046	7.151	NA
07-07-21C <>	409.864	4,403.060	0.895	19.584	4.013	0.238	5.251	0.034	3.386	0.645	214.177	7.132	216.652	10.244	243.656	92.516	214.177	7.132	NA
07-07-16C <>	369.005	83,420.569	0.989	19.822	2.706	0.236	2.942	0.034	1.155	0.392	214.675	2.438	214.764	5.695	215.745	62.672	214.675	2.438	NA
07-07-7C <>	1,766.257	101,433.027	0.803	19.731	0.963	0.238	1.950	0.034	1.695	0.870	215.965	3.601	216.840	3.807	226.362	22.269	215.965	3.601	NA
07-07-5C <>	160.727	52,113.987	0.947	19.785	6.587	0.239	6.775	0.034	1.585	0.234	217.752	3.394	217.943	13.289	220.002	152.543	217.752	3.394	NA
07-07-6C <>	574.462	153,060.936	0.831	19.764	2.038	0.243	2.480	0.035	1.414	0.570	220.553	3.065	220.725	4.920	222.556	47.130	220.553	3.065	NA
07-07-14C <>	705.414	14,144.051	1.108	19.456	1.878	0.247	3.407	0.035	2.843	0.834	220.913	6.174	224.188	6.854	258.725	43.155	220.913	6.174	NA
07-07-9C <>	409.478	99,234.036	0.719	19.443	2.158	0.250	2.618	0.035	1.483	0.566	223.281	3.254	226.514	5.316	260.238	49.579	223.281	3.254	NA
07-07-8C <>	94.338	11,318.562	0.974	22.815	13.423	0.215	13.613	0.036	2.267	0.167	225.048	5.014	197.493	24.436	-120.155	332.327	225.048	5.014	NA
07-07-20C <>	167.296	23,369.970	2.466	18.325	8.071	0.310	12.763	0.041	9.887	0.775	260.270	25.221	274.178	30.676	394.619	181.288	260.270	25.221	NA

Sample: 07-11	UTM N	6,669,913	UTM E	396,266	Unit	La Laguna Gabbro	Isotope ratios								Apparent ages (Ma)				
Analysis	U (ppm)	$^{206}Pb/^{204}Pb$	U/Th	$^{206}Pb^*/^{207}Pb^*$	± (1σ) (%)	$^{207}Pb^*/^{235}U^*$	± (1σ) (%)	$^{206}Pb^*/^{238}U$	± (1σ) (%)	error corr.	$^{206}Pb^*/^{238}U^*$	± (1σ) (Ma)	$^{207}Pb^*/^{235}U$	± (1σ) (Ma)	$^{206}Pb^*/^{207}Pb^*$	± (1σ) (Ma)	Best age (Ma)	± (1σ) (Ma)	Conc (%)
07-11-3 <>	96.884	13,839.968	0.870	19.846	7.889	0.238	8.632	0.034	3.503	0.406	216.814	7.469	216.482	16.830	212.857	183.002	216.814	7.469	NA
07-11-4 <>	87.449	10,004.645	0.869	19.348	9.460	0.245	10.207	0.034	3.834	0.376	218.151	8.225	222.737	20.417	271.442	217.259	218.151	8.225	NA
07-11-2 <>	78.947	14,457.891	0.855	19.711	28.310	0.241	28.783	0.034	5.199	0.181	218.293	11.159	219.179	56.802	228.702	665.815	218.293	11.159	NA
07-11-1 <>	120.868	7,682.238	0.852	20.363	11.025	0.234	11.456	0.035	3.114	0.272	219.145	6.709	213.608	22.072	153.017	258.896	219.145	6.709	NA
07-11-6 <>	444.310	58,841.510	1.625	19.503	2.663	0.291	3.111	0.041	1.609	0.517	260.229	4.105	259.522	7.125	253.122	61.245	260.229	4.105	NA
07-11-8 <>	1,147.112	14,043.702	0.883	19.179	0.958	0.297	2.286	0.041	2.075	0.908	261.213	5.313	264.283	5.319	291.610	21.903	261.213	5.313	NA
07-11-7 <>	1,353.111	76,206.624	0.506	19.350	0.718	0.298	1.648	0.042	1.483	0.900	264.531	3.845	265.216	3.847	271.255	16.467	264.531	3.845	NA
07-11-10 <>	1,509.211	367,283.663	0.506	19.332	0.676	0.301	1.619	0.042	1.471	0.909	266.102	3.834	266.851	3.799	273.409	15.471	266.102	3.834	NA
07-11-11 <>	1,193.445	747,143.109	0.572	19.375	0.873	0.300	2.121	0.042	1.933	0.911	266.331	5.042	266.526	4.971	268.219	20.011	266.331	5.042	NA
07-11-5 <>	300.162	40,103.777	0.856	19.364	3.556	0.301	3.829	0.042	1.420	0.371	267.132	3.716	267.390	9.001	269.633	81.578	267.132	3.716	NA
07-11-12 <>	1,487.838	98,379.183	0.420	19.421	0.719	0.302	3.641	0.042	3.569	0.980	268.219	9.376	267.668	8.567	262.846	16.508	268.219	9.376	NA
07-11-9 <>	1,655.944	869,523.205	0.439	19.390	0.672	0.302	1.955	0.042	1.836	0.939	268.298	4.825	268.111	4.608	266.462	15.451	268.298	4.825	NA

Appendix 2 continued.

Sample: 07-13	UTM N	6,695,942	UTM E	368,473	Unit	Los Tilos			Isotope ratios				Apparent ages (Ma)						
Analysis	U (ppm)	$^{206}Pb/^{204}Pb$	U/Th	$^{206}Pb^*/^{207}Pb^*$	± (1σ) (%)	$^{207}Pb^*/^{235}U^*$	± (1σ) (%)	$^{206}Pb^*/^{238}U$	± (1σ) (%)	error corr.	$^{206}Pb^*/^{238}U^*$	± (1σ) (Ma)	$^{207}Pb^*/^{235}U$	± (1σ) (Ma)	$^{206}Pb^*/^{207}Pb^*$	± (1σ) (Ma)	Best age (Ma)	± (1σ) (Ma)	Conc (%)
07-13-6C	122.956	16,219.997	0.971	18.815	10.280	0.323	10.386	0.044	1.476	0.142	277.830	4.014	284.010	25.736	335.194	233.524	277.830	4.014	NA
07-13-19C	202.892	42,041.932	3.206	19.048	3.660	0.320	4.676	0.044	2.911	0.622	278.616	7.937	281.680	11.503	307.168	83.377	278.616	7.937	NA
07-13-15C	31.043	7,419.947	1.136	19.546	32.102	0.315	32.279	0.045	3.371	0.104	281.201	9.275	277.673	78.576	248.051	756.467	281.201	9.275	NA
07-13-4C	152.286	11,104.759	1.232	19.352	4.461	0.318	6.045	0.045	4.080	0.675	281.882	11.252	280.715	14.828	270.977	102.323	281.882	11.252	NA
07-13-17C	20.730	2,561.782	0.781	1.633	1,818.470	3.777	1,818.489	0.045	8.442	0.005	282.089	23.302	1,587.835	NA	NA	NA	282.089	23.302	NA
40372	120.020	12,050.426	1.949	17.755	14.468	0.349	15.582	0.045	5.786	0.371	283.557	16.051	304.126	40.974	465.079	322.030	283.557	16.051	NA
07-13-11C	16.431	2,515.949	1.326	23.665	59.717	0.264	60.546	0.045	9.982	0.165	285.280	27.857	237.587	128.948	-211.199	1637.887	285.280	27.857	NA
07-13-7C	42.062	11,755.700	1.583	21.942	25.762	0.285	26.151	0.045	4.489	0.172	286.080	12.560	254.735	58.982	-24.763	632.888	286.080	12.560	NA
07-13-21C	58.974	11,281.330	0.620	19.720	16.956	0.319	17.389	0.046	3.856	0.222	287.279	10.834	280.855	42.691	227.671	394.253	287.279	10.834	NA
07-13-12C	120.917	27,547.249	1.080	19.795	8.835	0.319	9.392	0.046	3.188	0.339	288.778	9.003	281.230	23.075	218.920	204.776	288.778	9.003	NA
07-13-9C	541.302	105,283.938	3.079	18.835	2.319	0.338	2.591	0.046	1.156	0.446	290.626	3.284	295.334	6.639	332.749	52.560	290.626	3.284	NA
07-13-14C	35.486	6002.565	1.508	3.275	1,092.376	1.942	1,092.394	0.046	6.210	0.006	290.729	17.653	1,095.712	NA	3497.441	837.486	290.729	17.653	NA
07-13-1C	57.456	16,072.548	1.436	19.060	22.843	0.336	23.425	0.047	5.186	0.221	293.074	14.859	294.491	59.950	305.737	526.501	293.074	14.859	NA
07-13-20C	121.887	21,690.399	0.726	19.558	9.873	0.328	10.129	0.047	2.263	0.223	293.457	6.491	288.296	25.428	246.642	227.809	293.457	6.491	NA
07-13-16C	290.876	61,438.120	1.629	18.947	3.144	0.339	3.393	0.047	1.277	0.376	293.604	3.665	296.499	8.725	319.378	71.448	293.604	3.665	NA
07-13-2C	97.810	10,611.945	0.634	21.185	13.712	0.304	14.258	0.047	3.906	0.274	293.907	11.223	269.211	33.728	59.564	328.107	293.907	11.223	NA
07-13-3C	138.563	31,073.233	1.565	18.532	6.410	0.348	7.255	0.047	3.397	0.468	294.524	9.781	303.072	19.012	369.394	144.532	294.524	9.781	NA
07-13-5C	181.319	20,163.768	1.329	19.596	4.293	0.332	4.614	0.047	1.689	0.366	297.139	4.904	291.021	11.674	242.175	98.987	297.139	4.904	NA
07-13-13C	80.578	12,963.201	0.988	20.214	13.935	0.323	14.217	0.047	2.820	0.198	298.414	8.225	284.341	35.273	170.157	326.729	298.414	8.225	NA
07-13-18C	635.919	23,503.116	0.737	18.773	1.605	0.352	2.299	0.048	1.646	0.716	301.837	4.853	306.276	6.079	340.240	36.340	301.837	4.853	NA

Sample: 07-15	UTM N	6.697.056	UTM E	366.163	Unit	Guanta Unit			Isotope ratios				Apparent ages (Ma)						
Analysis	U (ppm)	$^{206}Pb/^{204}Pb$	U/Th	$^{206}Pb^*/^{207}Pb^*$	± (1σ) (%)	$^{207}Pb^*/^{235}U^*$	± (1σ) (%)	$^{206}Pb^*/^{238}U$	± (1σ) (%)	error corr.	$^{206}Pb^*/^{238}U^*$	± (1σ) (Ma)	$^{207}Pb^*/^{235}U$	± (1σ) (Ma)	$^{206}Pb^*/^{207}Pb^*$	± (1σ) (Ma)	Best age (Ma)	± (1σ) (Ma)	Conc (%)
07-15-5C	250.908	41,820.823	0.996	19.123	8.580	0.331	9.549	0.046	4.190	0.439	288.963	11.839	289.981	24.091	298.180	196.043	288.963	11.839	NA
07-15-15C	249.575	45,137.146	1.133	18.662	5.629	0.341	6.407	0.046	3.060	0.478	290.668	8.698	297.750	16.536	353.644	127.257	290.668	8.698	NA
07-15-19C	292.337	15,723.700	1.183	18.422	7.826	0.346	8.605	0.046	3.578	0.416	290.930	10.178	301.351	22.441	382.831	176.108	290.930	10.178	NA
07-15-2C	110.696	10,001.776	1.357	22.165	17.154	0.288	17.397	0.046	2.897	0.167	291.435	8.254	256.733	39.485	-49.346	419.981	291.435	8.254	NA
07-15-1C	321.081	24,118.195	1.270	19.589	8.250	0.326	8.387	0.046	1.508	0.180	291.800	4.303	286.454	20.935	243.079	190.368	291.800	4.303	NA
07-15-10C	152.248	18,706.675	1.411	17.969	9.811	0.358	10.051	0.047	2.183	0.217	294.013	6.274	310.770	26.915	438.445	218.844	294.013	6.274	NA
07-15-11C	125.606	13,759.028	2.395	18.505	16.745	0.348	16.876	0.047	2.099	0.124	294.506	6.043	303.433	44.291	372.633	379.341	294.506	6.043	NA
07-15-13C	224.630	19,968.112	0.995	18.699	6.423	0.345	7.305	0.047	3.480	0.476	294.698	10.023	300.882	19.024	349.153	145.340	294.698	10.023	NA
07-15-7C	267.170	33,670.104	1.151	18.784	9.044	0.345	9.144	0.047	1.348	0.147	295.979	3.898	300.862	23.814	338.891	205.211	295.979	3.898	NA
07-15-6C	205.778	12,501.551	1.056	18.561	26.819	0.350	27.216	0.047	4.634	0.170	296.461	13.427	304.424	71.705	365.887	614.428	296.461	13.427	NA
07-15-8C	119.598	24,130.599	1.279	19.457	18.505	0.335	19.428	0.047	5.917	0.305	297.456	17.200	293.110	49.502	258.624	428.370	297.456	17.200	NA
07-15-17C	214.018	13,915.640	1.406	20.821	12.670	0.313	13.058	0.047	3.162	0.242	297.493	9.192	276.320	31.599	100.644	300.666	297.493	9.192	NA
07-15-16C	295.131	52,174.856	1.099	20.126	4.415	0.325	4.836	0.047	1.972	0.408	298.664	5.755	285.636	12.040	180.304	102.956	298.664	5.755	NA
07-15-3C	202.838	25,802.183	0.940	17.740	4.186	0.369	4.895	0.047	2.538	0.518	298.949	7.414	318.852	13.396	466.959	92.753	298.949	7.414	NA
07-15-14C	659.555	66,015.665	1.725	18.960	3.931	0.346	4.174	0.048	1.404	0.336	299.722	4.112	301.787	10.897	317.763	89.389	299.722	4.112	NA
07-15-21C	236.955	39,389.526	1.025	18.603	5.217	0.358	6.822	0.048	4.396	0.644	304.447	13.071	311.051	18.280	360.828	117.766	304.447	13.071	NA
07-15-4C	255.354	29,094.497	1.006	18.835	7.606	0.356	9.272	0.049	5.302	0.572	305.945	15.843	309.072	24.711	332.756	172.688	305.945	15.843	NA
07-15-12C	611.629	45,825.626	0.546	19.368	4.387	0.347	4.800	0.049	1.947	0.406	306.520	5.827	302.223	12.547	269.157	100.656	306.520	5.827	NA
07-15-9C	199.728	19,383.507	1.340	19.952	7.880	0.339	9.153	0.049	4.657	0.509	308.430	14.024	296.174	23.518	200.613	183.209	308.430	14.024	NA
07-15-20C	264.327	40,886.438	1.391	19.819	5.680	0.344	10.288	0.049	8.578	0.834	310.857	26.032	299.972	26.726	216.090	131.600	310.857	26.032	NA
07-15-18C	222.452	23,096.990	1.308	18.484	9.506	0.375	10.556	0.050	4.590	0.435	316.413	14.174	323.550	29.256	375.212	214.350	316.413	14.174	NA